



A review on additive manufacturing of piezoelectric ceramics: From feedstock development to properties of sintered parts



Subhadip Bhandari^{a,*}, Gaurav Vajpayee^{b,c}, Lucas Lemos da Silva^b, Manuel Hinterstein^b, Giorgia Franchin^a, Paolo Colombo^{a,d,**}

^a Department of Industrial Engineering, University of Padova, Via Marzolo 9, Padova 35131, Italy

^b Fraunhofer IWM, Freiburg 79108, Germany

^c Institute for Applied Materials, Karlsruhe Institute of Technology, Karlsruhe 76131, Germany

^d Department of Materials Science and Engineering, The Pennsylvania State University, University Park, PA, USA

ARTICLE INFO

Keywords:

Additive manufacturing
Piezoelectric ceramics
 BaTiO_3
PZT
Debinding
Sintering
Dielectric

ABSTRACT

Piezoelectric ceramics are extensively used in several engineering applications in the field of sensors, actuators, energy harvesting, biomedical, and many more. Traditional ways of manufacturing piezoelectric devices result in better piezoelectric/ferroelectric performance. However, they are restricted to only simple shapes. With the widespread influence of additive manufacturing (AM), it is now possible to fabricate complex structures which were not possible by conventional technologies. In order to fabricate such complex structures with precision, it is necessary to understand in detail the factors influencing the feedstock preparation and the challenges associated with different AM technologies. With an emphasis on the most commonly used AM techniques (direct ink writing, fused filament fabrication, vat photopolymerization, binder jetting, and selective laser sintering) for

Abbreviation: d_{10} , 10 % of particles in the powder are smaller than this size; d_{50} , 50 % of particles in the powder are smaller than this size; d_{90} , 90 % of particles in the powder are smaller than this size; Ec, Critical energy density; T_c , Curie temperature; C_d , Curing depth; $\tan\delta$, Dielectric loss; T_g , Glass transition temperature; ϵ_r , Permittivity; d_{33} , Piezoelectric coefficient; P_r , Remanent polarization; G'_{eq} / G , Storage modulus; τ_y , Yield stress; ABS, Acrylonitrile Butadiene Styrene; ACMO, Acryloylmorpholine; $\text{Al}(\text{H}_2\text{PO}_4)_3$, Aluminium dihydrogen phosphate; AM, Additive manufacturing; APA, Ammonium salt of polyacrylic acid; APS, Average particle size; Ar, Argon; BaCl_2 , Barium chloride; BaCO_3 , Barium carbonate; BaO , Barium oxide; BAPO, Bis 2,4,6-trimethylbenzoyl-phenyl phosphine oxide; BaSnO_3 , Barium stannate; BaSrTiO_3 or BST, Barium strontium titanate; BaTiO_3 or BT, Barium titanate; BaZrO_3 , Barium zirconate; BCTZ, $(\text{Ba}_{0.85}\text{Ca}_{0.15})(\text{Ti}_{0.9}\text{Zr}_{0.1})\text{O}_3$; BCZT, Barium calcium zirconium titanium oxide; BEEA, 22-butoxyethoxy-ethyl acetate; $\text{Bi}_2\text{Mo}_2\text{O}_9$, Bismuth molybdate; BiFeO_3 , Bismuth ferrite; BIT, Bismuth titanate; BJ, Binder jetting; Ca, Calcium; CaTiO_3 , Calcium titanate; CNT, Carbon nanotubes; Co, Cobalt; CP, Ceramic particle; CuO, Copper oxide; DIW, Direct ink writing; DLP, Digital light processing; DMF, Dimethylformamide; DPPHA, Dipentaerythritol penta/hexa-acrylate; DTG, Derivative Thermogravimetry; Er, Erbium; ETPTA, Ethoxylated trimethylolpropane triacrylate; EVA, Ethylene vinyl acetate; F, Lotgering factor; FDC, Fused deposition of ceramics; FF, Fast firing; FFF, Fused filament fabrication; FS, Field strength; FTIR, Fourier transform infrared spectroscopy; HBA, 4-hydroxybutyl acrylate; HDDA, 1,6-Hexanediol diacrylate; HDODA, 1,6-Hexanediol; HNO_3 , Nitric acid; HPMC, Hydroxypropyl methylcellulose; IEP, Isoelectric point; KNN, Potassium sodium niobate; La, Lanthanum; Li, Lithium; LVR, Linear viscoelastic region; MDEA, N-methyl diethanolamine; MEHQ, 4-Methoxyphenol; DSC, Differential scanning calorimetry; Mn, Manganese; N₂, Nitrogen; Na, Sodium; Nb, Niobium; Nb_2O_5 , Niobium pentoxide; NH₄, Ammonium ion; NH₄Cl, Ammonium chloride; NH₄OH, Ammonium hydroxide; Ni, Nickel; OPPEOA, Oligo propylene glycol ethoxy triacrylate; PAA, Polyacrylic acid; PAA-NH₄, Ammonium polyacrylate; PAAS, Sodium polyacrylate homopolymer; Pb₃O₄, Lead (II,IV) oxide; PCL, Polycaprolactone; PE, Polyethylene; PEG, Polyethylene glycol; PEGDA, Polyethylene glycol diacrylate; PEI, Polyethylenimine; PEMA, Polyethyl methacrylate; PET, Polyethylene terephthalate; PFA, Pore forming agent; PI, Photoinitiator; PIN-PMN-PT, $\text{PbIn}_{1/2}\text{Nb}_{1/2}\text{O}_3\text{-PbMg}_{1/3}\text{Nb}_{2/3}\text{O}_3\text{-PbTiO}_3$; PLA, Polylactic acid; PMMA, Polymethyl methacrylate; PMN-PT or PMNT, Lead magnesium niobate-lead titanate; PNZT, Lead niobium zirconate titanate; POE, Phenoxyethanol; PP, Polypropylene; PPG, Polypropylene glycol; PPTA, Ethoxylated pentaerythritol tetraacrylate; PS, Polystyrene; PSD, Particle size distribution; P-SPS, Pressureless spark plasma sintering; PTC, Positive temperature coefficient; PTFE, Polytetrafluoroethylene; PUA, Polyurethane acrylate; PVA, Polyvinyl alcohol; PVB, Polyvinyl butyral; PVDF, Polyvinylidene fluoride; PVP, Polyvinylpyrrolidone; PZT, Lead zirconate titanate; RC, Robocasting; RH, Relative humidity; RI, Refractive index; RT, Room temperature; S, Strain; Sb, Antimony; SEM, Scanning electron microscopy; SLS, Selective laser sintering; SLA, Stereolithography; SrTiO₃, Strontium titanate; SS, Soluble starch; Ta, Tantalum; TCP, Tricalcium phosphate; TGA, Thermogravimetric Analysis; TiO₂, Titanium dioxide; TMPTA, Trimethylolpropane triacrylate; TPGDA, Tripropylene Glycol Diacrylate; TPMS, Triply periodic minimal surface; TPO, Diphenyl 2,4,6-trimethylbenzoylphosphine oxide; TPU, Thermoplastic polyurethane; TTIP, Titanium isopropoxide; UHS, Ultra-fast high temperature sintering; UV, Ultraviolet; VP, Vat photopolymerization; Zn(CH₃CO₂)₂, Zinc acetate; ZrO₂, Zirconia.

* Corresponding author.

** Corresponding author at: Department of Industrial Engineering, University of Padova, Via Marzolo 9, Padova 35131, Italy.

E-mail addresses: subhadip.bhandari@phd.unipd.it (S. Bhandari), pao.locolombo@unipd.it (P. Colombo).

fabricating ceramic parts, this review paper intends to provide a deep insight into the factors affecting the feedstock preparation as well as post-processing conditions required to develop a high-performance piezoelectric device. The summarized tables detailing the various piezoelectric ceramic compositions and additives or ingredients used in formulating a printable feedstock, along with the optimum printing and post-processing conditions, will aid the readers in developing their own printable formulations and determining the best post-processing parameters to achieve the best performance out of the fabricated piezoelectric device. The advantages and disadvantages of the AM technologies are analyzed with specific reference to piezoceramic materials and the remaining challenges that require further research are emphasized. Furthermore, with the ongoing and continuous developments in additive manufacturing of piezoelectric materials, it is expected that such advancements will progressively transition towards commercialization, with the ultimate goal of widely incorporating additively manufactured devices into practical applications.

1. Introduction

Global energy consumption expanded considerably during the last half-century due to industrialization, technological advancements and population growth. It approximately doubled between 1971 and 2019, reaching 14,421 Mtoe (million tons of oil equivalent) in 2019 [1]. This rising demand highlights the critical need for long-term energy solutions based on materials that can efficiently harness, store, and transform energy. A wide range of functional materials including ceramics, polymers and composite materials can be used to meet such requirements [2]. However, among these options, piezoelectric ceramics stand out due to their intrinsic properties, such as high permittivity, robust mechanical strength, high-temperature stability and excellent electromechanical coupling coefficients [3].

When subjected to mechanical stress, piezoelectric ceramics generate an electric charge, directly converting mechanical energy into electrical energy and vice versa. The most common and traditionally used piezoelectric material belongs to the family of lead zirconate titanate (PZT) due to its superior piezoelectric coefficient (d_{33}) [4]. However, the use of lead is considered dangerous due to health and environmental hazards as well as concerns regarding recycling and disposal [5]. Following this, in the year 2002 legislations were introduced in the European Union, governing the use of lead and other harmful elements in commercial products [6,7]. The restriction on using such hazardous substances has emphasized the urgency to eliminate lead from these ceramics. Environmental concerns associated with lead have driven research towards lead-free alternatives [8–11]. Materials such as barium titanate (BaTiO_3 or BT), BT-based solid solutions such as BT doped with calcium and zirconium (BCZT), potassium sodium niobate (KNN) and bismuth ferrite (BiFeO_3) etc., are being researched intensively as a potential alternative to PZT [12]. Although there have been advancements in lead-free compositions, it is important to note that these ceramics still do not possess the same level of high piezoelectric characteristics as PZT ceramics.

Subsequently, further research efforts were aimed at enhancing the piezoelectric characteristics of lead-free compositions. The strategies to achieve better piezoelectric properties include microstructure optimization, texturing and addition of suitable dopants [12]. The dielectric and piezoelectric characteristics are significantly influenced by the grain size [13–16] as well as the domain size [17]. A ferroelectric domain is a region of a ferroelectric material in which the spontaneous electric polarization is oriented in a specific direction [18]. For example, BT exhibits optimum piezoelectric properties when the grain size is in the order of 1 – 2 μm with domain sizes of around 100 nm [16,19–22]. In contrast, decreasing the grain size below 100 nm induces a paraelectric state [23,24]. In addition, texturing also helps in enhancing the piezoelectric and dielectric characteristics by increasing the proportion of domains aligned in the direction of the electric field [25]. Ceramics with templated-grain growth along certain directions such as [001], [110] and [111] have been reported to exhibit better piezoelectric properties than randomly oriented polycrystalline materials [26–28]. One of the most widely exploited techniques to enhance the piezoelectric properties to date is the addition of dopants which substitute the A- or B-site

cations [12]. A summary of promising doped BT compositions with d_{33} more than 200 pC/N has been reported in the literature [12].

A wide range of conventional ceramic processing technologies such as slip casting [29], tape casting [30], die pressing [31], injection molding [32], etc. have been utilized to fabricate piezoceramics. However, these conventional techniques have certain limitations. These include time-consuming manufacturing processes, extremely high wear rates of expensive machining tools, difficulties in producing complex geometries with high accuracy, and related high labour costs [33]. Additionally, the mechanical stress applied during the conventional processing techniques often leads to grain loss, strength degradation and depolarization of the near-surface area in piezoelectric elements [34]. This deterioration significantly impacts the overall performance of the fabricated component. A solution to these problems came with the evolution of innovative three-dimensional (3D) printing technologies or additive manufacturing (AM) that enables the manufacture of complex structures with high accuracy and increased production costs. Perhaps the most important reason for resorting to AM techniques is the promise of creating shapes that may increase the functional value beyond what is currently possible with conventional ceramic fabrication methods [35].

The AM technologies for metallic and polymeric components have grown and developed significantly in the last several years. In fact, these technologies have now been commercialized and are ready to be used in industrial applications. On the contrary, the use of AM technologies in the field of ceramics has been sluggish [36]. The present technical delay may be attributed to the intricate nature of ceramics processing rather than a lack of technological enthusiasm. Indeed, one might argue that AM has particular advantages for the fabrication of ceramics compared to any other material families. When considering ceramics, justifications for using AM are particularly compelling due to the challenges posed by their inherent hardness and brittleness. These challenges limit the feasibility of subtractive manufacturing methods, making 3D printing a viable alternative for enhancing and broadening the range of applications for functional ceramics.

Fig. 1(a) reports the most widely used AM technologies concerning piezoelectric ceramics over the past 20 years. This includes vat photopolymerization (VP), direct ink writing (DIW), fused filament fabrication (FFF), binder jetting (BJ), and selective laser sintering (SLS) [35]. **Fig. 1(b)** illustrates the distribution of research publications that have been published to date, categorizing them according to the various AM techniques. The distribution of research publications demonstrates how widely in particular VP and DIW are being used, which highlights their importance in pushing the boundaries of AM for piezoelectric ceramics. In terms of materials, there has been a progressive shift from lead-based compositions to lead-free compositions including pure BT, doped BT, KNN, BCZT, etc., as depicted in **Fig. 1(c)**. One can also clearly notice in **Fig. 1(a)** that SLS is a single-step process, eliminating the need for an additional debinding step before sintering, unlike the other techniques reviewed here.

Several review articles have been published to date on the additive manufacturing (AM) of piezoceramics, as reported in **Table 1**. These papers primarily focus on various AM technologies related to piezoceramics and discuss the piezoelectric and ferroelectric properties of the

fabricated components. However, an essential aspect of additive manufacturing – the preparation of the feedstock and the factors influencing it, has not been adequately addressed in any of the existing review papers. Additionally, the different factors influencing the functional properties of these materials are also missing. Further, there have been significant developments and achievements in the past couple of years involving AM of piezoceramic materials that need to be highlighted to the research community.

In this aspect, this review paper aims to summarize the latest state of the art of research concerning AM of piezoelectric ceramics, with a major focus on the feedstock development, which is a key parameter for the success of the fabrication process. In fact, the structural integrity and the quality of the final fabricated component mostly depends on the preparation of the feedstock, hence plays a vital role in the complete fabrication process chain. Additionally, we discuss the piezoelectric and ferroelectric characteristics of the sintered components and analyze how these characteristics are influenced by variations in density, microstructure, and design. A comprehensive analysis of the additive manufacturing techniques specifically applied to the fabrication of piezoceramic components has also been carried out. It is important to mention that this review study only focuses on research papers that include debinding and sintering of piezoelectric ceramics after the fabrication. However, recent studies on FFF technology lacks sufficient investigation into pure ceramics (Tables 3, 9), resulting in the inclusion of polymer-ceramic composites in the review.

Table 1
Review papers published on AM of piezoceramic materials.

Sl. No.	Year of publication	Title	Reference
1	2020	Additive Manufacturing of Piezoelectric Materials	[35]
2	2020	Progress and challenges of 3D-printing technologies in the manufacturing of piezoceramics	[2]
3	2022	A Review on Additive Manufacturing of Functional Gradient Piezoceramic	[37]
4	2023	A Review on Recent Advances in Piezoelectric Ceramic 3D Printing	[38]
5	2023	Review of the applications of 3D printing technology in the field of piezoelectric ceramics	[39]

2. Additive manufacturing (AM)

2.1. Direct ink writing (DIW) / Robocasting (RC)

2.1.1. Basics of the technology

Direct ink writing (DIW) or robocasting (RC) is an extrusion-based AM technique in which a non-newtonian viscous ceramic ink with suitable viscoelastic properties is extruded through a nozzle and deposited on the print bed following the printing path at room temperature. It is one of the most widely used AM technology, thanks to its flexibility, simplicity, and cost-effectiveness in fabricating relatively

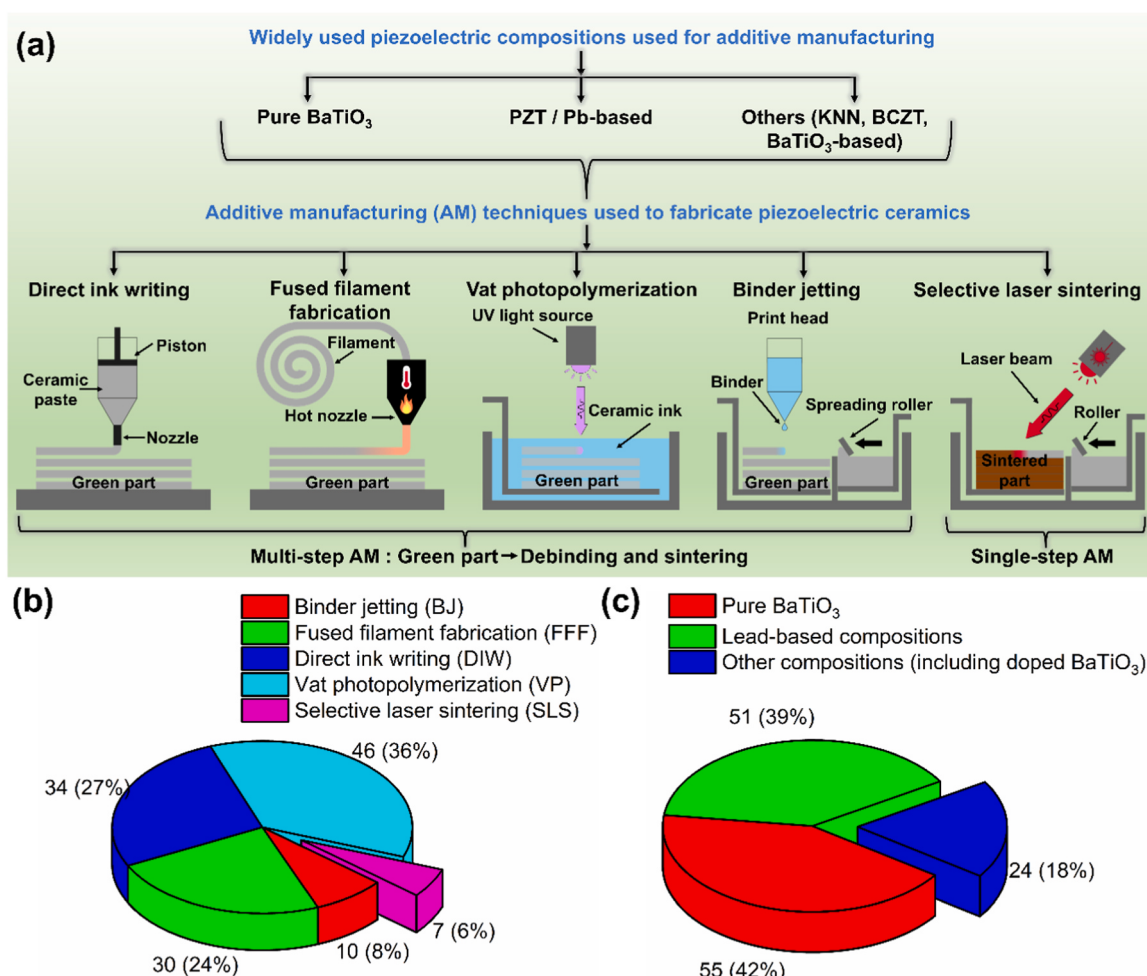


Fig. 1. (a) Overview of the piezoelectric compositions and the additive manufacturing techniques used to fabricate them. Graphical representation of: (b) Research papers reviewed in this study, categorized by the most widely used AM technologies, and (c) Various piezoelectric materials used with different AM technologies.

simple geometries and larger structures, without the need of ultraviolet (UV) curing or laser radiation [33,40]. These features significantly broaden the versatility in the range of powders that can be utilised as it is independent on the optical properties of the starting powder or the laser power required for consolidation. Additionally, DIW allows preparation of small amounts of ink, thereby minimizing the waste and making it more efficient. However, this comes at the expense of poor accuracy and surface finish, as it is constrained by the nozzle diameter (mostly $> 400 \mu\text{m}$ as evidenced in Table 2) which limits the resolution of the printed components. Ceramic inks for such extrusion-based processes demand high ceramic loading ($> 50 \text{ vol\%}$) with a suitable solvent and appropriate amount of additives such as dispersant, coagulant, binder and humectant (solvent trap) [41]. High ceramic loadings in the ink are often associated with nozzle clogging and rapid drying of the ink, therefore limiting the upscaling of this technology.

One of the primary prerequisites for having a smooth flow of ink through the nozzle is the use of ink with optimized rheological properties [41,42]. The ink should possess a suitable viscoelastic behaviour; viscous when stress is applied so that it can easily exit from the nozzle without employing high pressure and, once the ink is extruded, it should have sufficient viscosity to keep the integrity of the fabricated structure without deformation or sagging, linked to the elastic part.

Maintaining tight control over the rheology of DIW pastes is crucial in order to manufacture printed ceramics of superior quality. It is thus of the utmost importance to review the factors that influence the rheology of the prepared ceramic ink.

2.1.2. Effect of zetapotential and pH

Most of the lead-free and lead-containing piezoceramics are highly sensitive to water, usually undergoes hydrolysis and dissolution [43–46]. This leads to: 1) leaching of metallic ions into the solution, and 2) reprecipitation of the leached metallic ions thereby affecting the stoichiometry. The concept of ion leaching is somewhat related to the ionic field strength (FS), which considers the charge and size of the concerned ion, defined as [47]:

$$FS = \frac{\text{ionic charge}}{\sqrt{\text{ionic radius}(\text{\AA})}} \quad (1)$$

The lower FS, the easier is the dissolution due to weak bonding and vice versa. These solid-liquid interactions impose restrictions on the maximum solid loading that can be achieved and result in unstable suspensions that are unsuitable for further ink production and storage. All of these issues can be easily solved by either adjusting the pH value or by the addition of surfactants.

The stability of colloidal suspensions is dictated by the zeta potential of the solid particles in the solution. This parameter serves as an indicator of the magnitude of electrostatic forces, either repulsive or attractive, that exist between particles within a dispersion. A common way to figure out the stability of a colloidal solution is to look at how the zeta potential changes with pH. Generally speaking, a high zeta potential indicates that particles are highly charged (positive, 30 mV or negative, -30 mV) and repel each other, thereby stabilizing the dispersion [48]. It is interesting to note that the plot passes through a value of 0 zeta potential (as shown in Fig. 2(a, c)) known as the iso-electric point (IEP), indicating that in those conditions the suspension is least stable with a high possibility of aggregation or flocculation. Lower zeta potential values (in between 30 mV to -30 mV) may also cause such instabilities.

When employing a ceramic ink for robocasting, which requires a stable and smooth flow of ink with high solid loading through the nozzle, it is important to understand the correlation between zeta potential and pH in order to achieve and maintain the stability of colloidal suspensions. In order to accomplish a homogeneous dispersion of the pure BT and polyacrylic acid (PAA)-coated BT nanoparticles, Li *et al.* studied the variation of zetapotential as a function of the pH [49]. The

zeta potential measurement revealed that the BT particles are positively charged and PAA-coated BT particles are negatively charged at pH 9 (Fig. 2(a)). Electrostatic interaction between opposing charges causes PAA to adsorb onto BT particles, thereby stabilizing the suspension. In addition, the iso-electric point also shifts to lower pH after addition of PAA; similar behaviour has been also reported for BT powder coated with ammonium polyacrylate (APA) [50] and BCZT powder coated with aluminium dihydrogen phosphate ($\text{Al}_2(\text{H}_2\text{PO}_4)_3$) [51]. Such shift in the iso-electric point indicates that the surface modifiers are effective in promoting stability within the suspension.

The stability of the surface treated powder as a function of time was further investigated by Nan *et al.* [51]. The untreated and treated BCZT powders were subjected to an aging period of 64 h, during which pH values were measured. It was observed that the pH values of the treated powder remain almost constant with highly homogeneous dispersion (left image in Fig. 2(b)). In contrast, the untreated powders demonstrated inadequate wetting (caking) and significant agglomeration with increasing pH value with aging period (right image in Fig. 2(b)). The untreated powder in contact with water undergoes dissolution reaction and the rate of ion leaching is determined by the ionic field strength values which follows the order: $\text{Ba}^{2+} > \text{Ca}^{2+} > \text{Zr}^{4+} > \text{Ti}^{4+}$. This means that, for every divalent ion leached into the water, there is a simultaneous uptake of H^+ ions to maintain the electroneutrality. So, the increasing pH is due to the absorption of H^+ ions from the solution in order to maintain electro-neutrality, leading to an imbalance between H^+/OH^- ions.

In contrast to BT and BCZT, PIN-PMN-PT ($\text{Pb}(\text{In}_{1/2}\text{Nb}_{1/2})\text{O}_3\text{-Pb}(\text{Mg}_{1/3}\text{Nb}_{2/3})\text{O}_3\text{-PbTiO}_3$) exhibits a dual IEP characteristic, as shown in Fig. 2(c) [52]. Such duality imposes complexity in the system. The complex metal oxides involved in PIN-PMN-PT are incongruent as a function of pH [53]. The addition of an acrylic-based binder causes the particles to lose their dual iso-electric point and the suspension is stabilized at a pH of 5 ($\sim -25 \text{ mV}$). At pH 12, the zeta potential value is no longer affected by the presence of PAA chains and the value is almost same for the pure powder and the powder with the acrylic binder.

Several studies have reported the variation of the rheological properties as a function of pH. For instance, Li *et al.* observed that for PZT ink lower pH led to suitable viscoelastic properties for a smooth extrusion process [54]. In another study, the effect of the pH on rheological and extrusion behaviour was also reported for PIN-PMN-PT ink [52]. The ink prepared at pH 1 and 13 were found to be almost identical, characterized by a high storage modulus, yield stress and inconsistent flow of the ink through the nozzle (Fig. 3(a)). It has been claimed that PAA exists in many configurations and has varying net charges depending on the pH [55]. At a lower pH, PAA is reported to exist in globular configuration without possessing any overall charge and the PIN-PMN-PT powder has positive zeta potential values. As a result, the PAA does not interact with the powder, thereby leading to flocculation. However, at higher pH levels, PAA chains are unfolded with negative charges on it and the powder has negative zeta potential values. Repulsion between ceramic particles and PAA chains create a homogenous dispersion. At the same time, the hydrogen bonding between the ionized PAA chains dominate [55], resulting in enhanced rheological properties. In contrast to the ink formulated at pH 1 (Fig. 3(b)) and 13, the ink prepared at pH 5 demonstrated the capability of being extruded into filaments with a uniform width (Fig. 3(c)). While the inks at pH 1 and 13 exhibited a gradual decrease in storage modulus, the pH 5 ink showed a sharp decrease, suggesting more effective interactions of PAA with the powder at pH 5. This is evident from the analysis in Fig. 3(a), where the yield stress decreased from over 1400 Pa to 530 Pa .

A study on the shape retention ability of a calibration (V-shaped) structure with spanning elements was carried out by Smay *et al.* [56]. The authors observed that the rheological properties were strongly affected by the change in pH. The ink with a pH of 8.05 ($G'_{eq} = 27 \text{ kPa}$, $\tau_y = 3 \text{ Pa}$) showed significant deformation even at small spanning lengths

Table 2

Feedstock preparation and optimized printing parameters for Direct ink writing (DIW).

Feedstock	Particle size and morphology	Solvent	Additives	Ceramic loading	Ink type	Printing parameters			Reference
						Nozzle size (mm)	Speed (mm/s)	Layer height (mm)	
PIN-PMN-PT	Monomodal, $d_{50} = 280$ nm Width: 2 – 40 μm , Thickness: 0.5 – 1 μm	Distilled water	WB4101, PL008, DS001, DF002, CuO (< 50 nm), HNO ₃ /NH ₄ OH	28 – 35 vol%	Colloidal	5			Extrusion pressure: 880 – 1250 kPa, Samples dried in 95 % R.H for 4 days [52]
BaTiO ₃ platelet									
Hard PZT	$d_{50} \sim 0.60$ μm	Distilled water	DISPERBYK-180, Glycerol, PVA	50 – 55 vol%	Colloidal	0.15 – 0.90	0 – 10	$\frac{h}{D} \sim 1$	Extrusion pressure: 0 – 0.20 MPa, Samples dried in 80 °C for 12 h [74] ^a
Barium acetate, TTIP		Isopropyl, Triple distilled water, Acetic acid, Isopropanol	BaTiO ₃ (> 3 μm)	30 – 80 wt%	Sol-gel	1.5	5 – 30	$\frac{h}{D} \sim 0.8$	Heated bed: 50 °C [78]
BaTiO ₃ Hydrothermally synthesized BCZT	Nano particles	DMF	PVDF	65 – 80 wt%	Colloidal	0.26, 0.41	~ 2.7		Extrusion pressure: 0.8 – 1 MPa, Samples dried in 80 °C for 6h, Printed on PET film [69]
BaTiO ₃	Bi-modal, $d_{50} = 0.17$ μm , $d_{90} = 0.38$ μm	Deionized water	Al(H ₂ PO ₄) ₃ , Dispex A40, HPMC, PEI	40 – 44 vol%	Colloidal	0.41			Samples dried in 40 °C for 8h, Printed in glycerin oil [51,84]
	$d_{50} = 1.2$ μm	Distilled water	Bermocol E 320 FQ, Darvan 821-A, PEI	50, 52 vol%	Colloidal	Square 1.5	5	1.35	
BaTiO ₃	100 nm, 300 nm, 500 nm	Deionized water	PVA	28.5 vol%	Colloidal	1	10	0.6	Printed in oil bath, Samples dried at RT °C for 24 h [70]
	100 nm, 300 nm	Deionized water	PVA	70 wt%	Colloidal	0.8 – 1.6	10 – 20		Printed on aluminum plate at –40 °C, Samples dried in –60 °C for 2h, Samples dried in 40 °C for 24 h [58]
BaTiO ₃ doped La, Mn PTC		Deionized water	Darvan 821-A, HPMC	33, 43 vol%	Colloidal	0.56	5	0.40	Print bed 20 – 80 °C, PTFE spray on print bed [71]
PZT		Deionized water	PVA, Trisodium citrate, Polyacrylamide, glycerol	86.21 wt%	Colloidal	0.5	8		Extrusion pressure: 0.2 MPa [85]
BaTiO ₃	15 – 60 nm Nano particles	Deionized water	PAA, Cellulose, NH ₄ Cl, Zn(CH ₃ CO ₂) ₂ , NH ₄ OH/ HNO ₃	50 vol%	Colloidal	0.03 – 0.1	1	0.9D	Printed in oil bath [49]
BaTiO ₃	APS = 1.02 μm	Deionized water	NH ₄ OH/ HNO ₃ , BaCl ₂ , APA, HPMC, PEI	49 vol%	Colloidal	0.1 – 0.5			Printed in oil bath, Samples dried at RT for 12 h [50]
Bi ₂ Mo ₂ O ₉	APS < 10 μm	Distilled water	Ethylene glycol diacetate, Propylene carbonate, Ethyl cellulose, Diisononyl phthalate, Ammonium lauryl sulphate	85 wt%	Colloidal	0.5	5	0.2	Samples dried at RT for 24 h [60]
BaTiO ₃	100 nm, 400 nm	Distilled water	PVA, PAA	28.5 vol%	Colloidal	0.6			Extrusion pressure: 58 MPa, Samples dried at –5 °C for 24 h and 40 °C for 24 h [61]
PZT	Spherical agglomerates of 0.5 μm particles	Deionized water	PVA	86 – 89 wt%	Colloidal	1.5	10	0.8	Print bed 40 °C, Samples dried in 40 °C for 8 h [77]
PZT	APS = 0.225 μm , spherical	Xylene, Ethanol	Triethyl phosphate, PEG, PVB	79 – 80.5 wt%	Colloidal	0.21 – 0.26			Samples dried at 60 °C for 1 h [72]
PIN-PMN-PT	Monomodal, $d_{50} = 280$ nm	Distilled water	WB4101, PL008, DS001, DF002	28 vol%	Colloidal	Customized nozzles	5, 10, 20		Extrusion pressure: 275 – 1100 kPa [91] ^b

(continued on next page)

Table 2 (continued)

Feedstock	Particle size and morphology	Solvent	Additives	Ceramic loading	Ink type	Printing parameters			Reference
						Nozzle size (mm)	Speed (mm/s)	Layer height (mm)	
BaTiO ₃ platelet	Width = 2 – 40 µm, Thickness = 0.5 – 1 µm			2.6 vol% of total paste					
BaTiO ₃ , SrTiO ₃ , BaZrO ₃ , Ni Nb, Ca, Co- doped BaTiO ₃		Deionized water	APA, HPMC, PEI	47 vol%	Colloidal				[92]
Nb, Ca, Co- doped BaTiO ₃	Mean diameter = 0.5 µm	Terpineol	BEEA, PEG, PVB	80 wt%	Colloidal	1	2 – 3		[80]
TTIP, MDEA, Glycerol, Water, BaO			BaTiO ₃	30 – 40 vol%	Sol-gel	0.41	5		Extrusion pressure: 40 kPa [73]
BaTiO ₃	$d_{50} \sim 1.05 \mu\text{m}$, spherical	Paraffin oil, mineral spirits, Stearin wax	Sucrose solution	31 vol%	Capillary suspension	0.15	10	0.12	Extrusion pressure: 480 kPa, Printed on porous alumina plate, Samples dried at RT for 5 days [88]
PZT	$d_{50} = 523 \text{ nm}$	Ethanol	Trisodium citrate, PVA, PAA-NH ₄ or PAAS, Glycerin		Colloidal	0.6	8	0.3	Extrusion pressure: 0.2 MPa [83]
BaCO ₃ , TiO ₂ PZT PZT95/5		H ₂ O	PVA, PEG 400, Solperse 20000	~ 75.1 wt%	Colloidal				[93]
	$APS = 0.5 \mu\text{m}$	Deionized water	AG 165, Methylcellulose	52 vol%	Colloidal	0.26			[54]
	$d_{50} = 1.25 \mu\text{m}$, $d_{max} = 4.50 \mu\text{m}$	Deionized water	PVP		Colloidal	0.30			Extrusion pressure: 0.3 MPa Samples dried at 60 °C for 24 h [94]
PNZT	Bimodal size distribution of 1.8 and 4.5 µm	Terpineol	Polyenoic acid, Phosphate ester, Fatty acid, Fatty acid ester, Ethyl cellulose	35 vol%	Colloidal	8 mils			[75]
Li, Sb, and Ta- doped KNN	$APS = 0.5 \mu\text{m}$	Methyl methacrylate, Pentaerythritol three acrylate		56 wt%	Colloidal	0.25 – 0.40			[95]
BaTiO ₃	500 nm	DMF	PVDF	25.85 –35.45 vol%	Colloidal	0.60	1	0.4	Printed on heat bed, Samples dried at 120 °C for 2 h [86]
BST and β-TCP		Water	PVA		Colloidal	0.2	11 – 13		Extrusion pressure: 3.8 – 4 bar [96]
BCTZ 50	$d_{50} = 1 \mu\text{m}$	Water	Dispex®AA4040, HPMC, PEI	41 vol%	Colloidal	0.25			Samples dried at RT for 24 h [97]
PZT		Deionized water	Polyacrylate, Cellulose, HNO ₃	32 vol%	Colloidal	0.41	5		Printing bed cooled below –25 °C, Freeze dried in vacuum chamber for 24 h [98]
PZT	$APS = 0.64 \mu\text{m}$	Deionized water	PAA, Cellulose, NH ₄ OH and HNO ₃	47 vol%	Colloidal	0.1 – 1	2 – 8	0.82D	Printed in oil bath, Sample dried at 30 % R.H at 23 °C [56]
BaTiO ₃		Distilled water	Na-PAA, Na-alginate, Glycerol	80 wt%	Colloidal	0.41			Extrusion pressure: 2–3 bar, Samples dried at RT for 4 h [79]

^ah is the strut height and D is the nozzle diameter. ^bThe nozzles were 24 mm long and had 6 mm diameter circular inlets which taper to elliptical outlet cross-sections of 580 µm x 580 µm (aspect ratio 1), 870 µm x 430 µm (aspect ratio 2), 750 µm x 250 µm (aspect ratio 3), and 1560 µm x 300 µm (aspect ratio 5). Tapered nozzles were used to reduce the printing pressure necessary to print continuous filaments. Nozzles with aspect ratios greater than 1 were custom made via stereolithography (3DSystems, State College, PA).

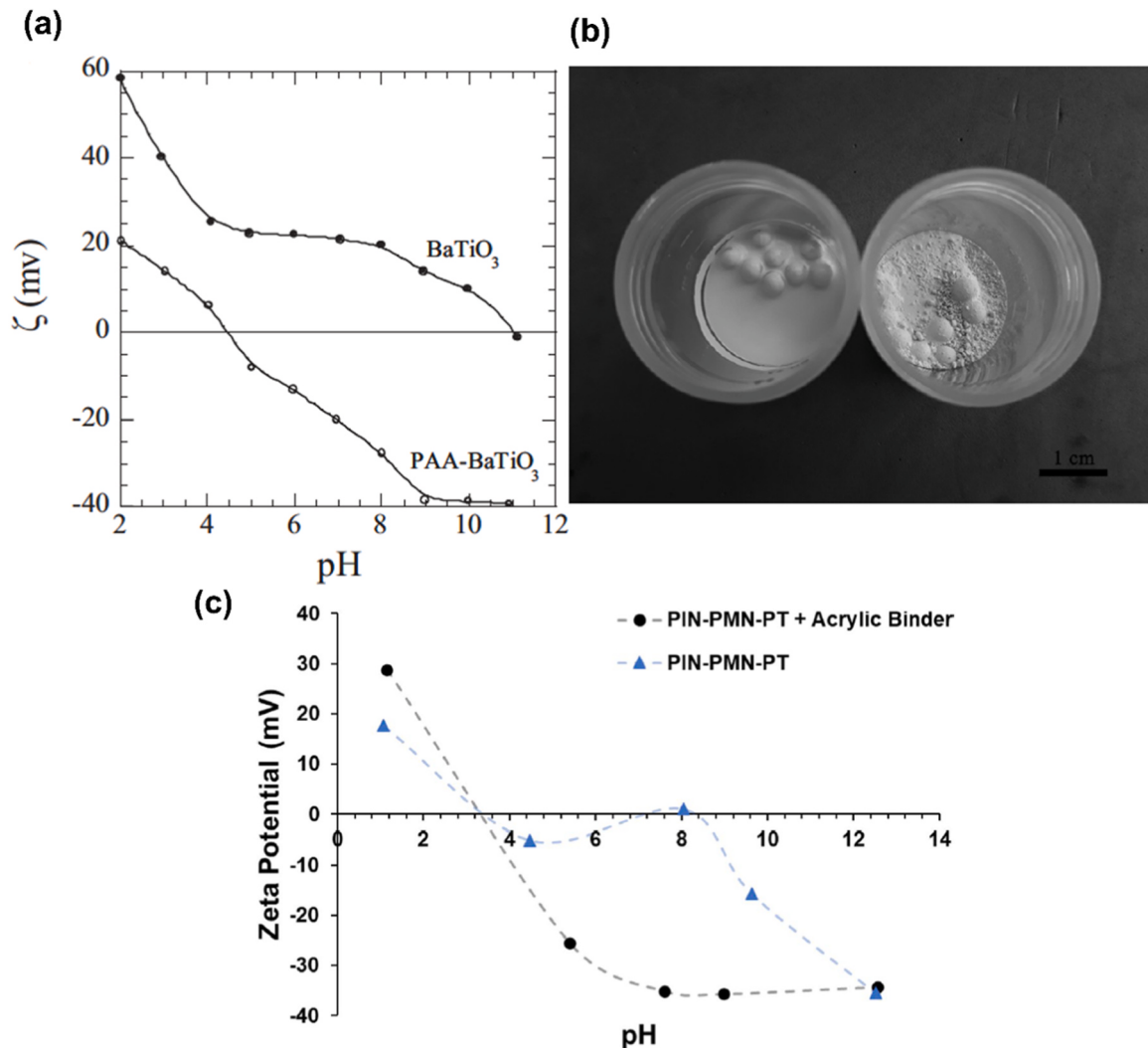


Fig. 2. Effect of the zeta potential and pH on the formulated ceramic ink. (a) Zeta potential variation of pure BT and PAA-coated BT as a function of different pH levels [49]. (b) The effect of surface treatment on the dispersibility of 40 vol% BCZT powders in the presence of 1.0 wt% dispersant made from the surface-treated powder (left) and the untreated powder (right) under the identical mixing conditions [51]. (c) Zeta potential as a function of pH for 0.08 vol% PIN-PMN-PT suspensions, with and without an acrylic binder [52].

Reproduced from Ref.: (a) [49], (b) [51], and (c) [52] with permission from John Wiley and Sons.

(Fig. 3(d)). With decreasing pH, the shape retention ability increased due to increasing viscosity, storage modulus and the yield stress, with the least deformation values being reported at a pH of 6.15 ($G'_{eq} = 150$ kPa, $\tau_y = 25$ Pa).

The pH of the ink has a significant impact on the surface charge of particles and the conformation of organic molecules. Consequently, depending on the interaction between the additives (surface modifier, dispersant, binder) and the ceramic powder, this may lead to a substantial deterioration of the properties such as increase/decrease in the viscosity, storage modulus and yield stress of the formulated ink, thereby affecting the shape retention capability of the ink. Regardless of the specific powder being used, it is important to determine the IEP and study the variation of the zeta potential, particularly for perovskite-structured powders that are susceptible to hydrolysis. The situation becomes further challenging when there is more than one IEP, as in the case of PIN-PMN-PT powders.

2.1.3. Effect of salt solution

In DIW, salt solutions have been sometimes used to induce gelation by cross-linking with the polymers used in the ink. Despite its effectiveness, this approach is no longer used by researchers because of post-

processing challenges that include removal of residues from the salt solution after the printing.

Li *et al.* used two distinct salt solutions, each containing either a monovalent (NH_4^+) or divalent (Zn^{2+}) salt species, that facilitated the transition from fluid to gel with the desired viscoelastic response for a highly loaded BT suspension, as shown in Fig. 4(a) [49]. A noticeable discrepancy was observed in the elastic modulus, with a substantial increasing modulus by orders of magnitude in the presence of divalent ions as opposed to monovalent ions (Fig. 4(b)). Monovalent counterions such as NH_4^+ can only neutralize the negative charge of COO-groups of PAA; on the other hand, divalent counterions like Zn^{2+} have the ability to facilitate aggregation by means of “ion-bridging” interactions between charged PAA chains that are adsorbed on the BT nanoparticles. Such increase in elastic behaviour on additions of the ions (monovalent or divalent) can also be related to the inter-particle bonding using a power law scaling relation [57]:

$$y = k \left(\frac{\phi}{\phi_{gel}} - 1 \right)^x \quad (2)$$

where y is the desired elastic property (such as yield stress or elastic modulus), k is a system specific constant, ϕ_{gel} is the minimum particle

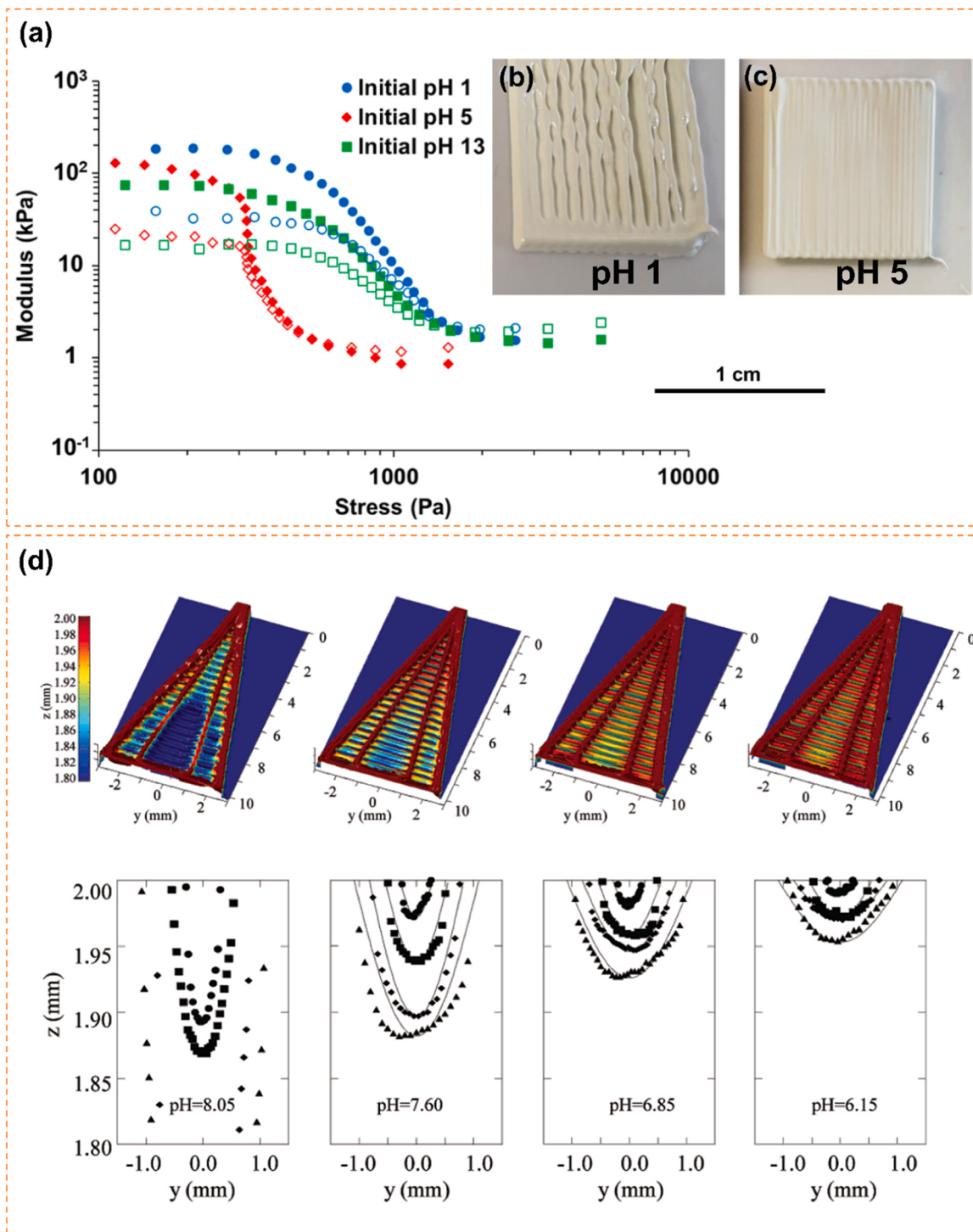


Fig. 3. Effect of the pH on the structural stability of the extruded ceramic ink. (a) Storage modulus (filled points) and loss modulus (hollow points) of 28 vol% PIN-PMN-PT pastes as a function of applied stress, formulated at various pH levels using a PAA binder system. Printing tests conducted with the same pastes prepared at (b) pH 1, and (c) pH 5 [52]. (d) Specific height profiles of test structures extruded from PZT colloidal gels for spans of approximately 3 mm (●), 5 mm (■), 7 mm (◆), and 9 mm (▲), at pH levels: 8.05, 7.60, 6.85, and 6.15. The colour scale indicates height between 1.8 and 2 mm [56].

Reproduced from Ref.: (a-c) [52], with permission from John Wiley and Sons. (d) [56], with permission from American Chemical Society.

loading necessary for gelation and ϕ is the solid volume fraction. The inter-particle interactions become more intense with increasing salt concentration, as a result ϕ_{gel} decreases (for a fixed ϕ) resulting in increased elastic properties. Further, addition of divalent salt solutions ($[Zn^{2+}] = 0.06$ M) promotes the fluid to gel transformation with optimum elastic behaviour ($G > 10^4$ Pa) necessary for shape retention. Such concentration of Zn^{2+} ions help in the transformation of long-range van

der Waals interactions to ion bridging effects, which in turn promotes stronger particle interaction leading to an increasing yield stress and elastic modulus of the ink. Nadkarni *et al.* observed similar results on addition of NaCl and BaCl₂ solution to APA-stabilized BT [50]. The magnitude of the rise in modulus was reported to be amplified in the presence of bivalent ions.

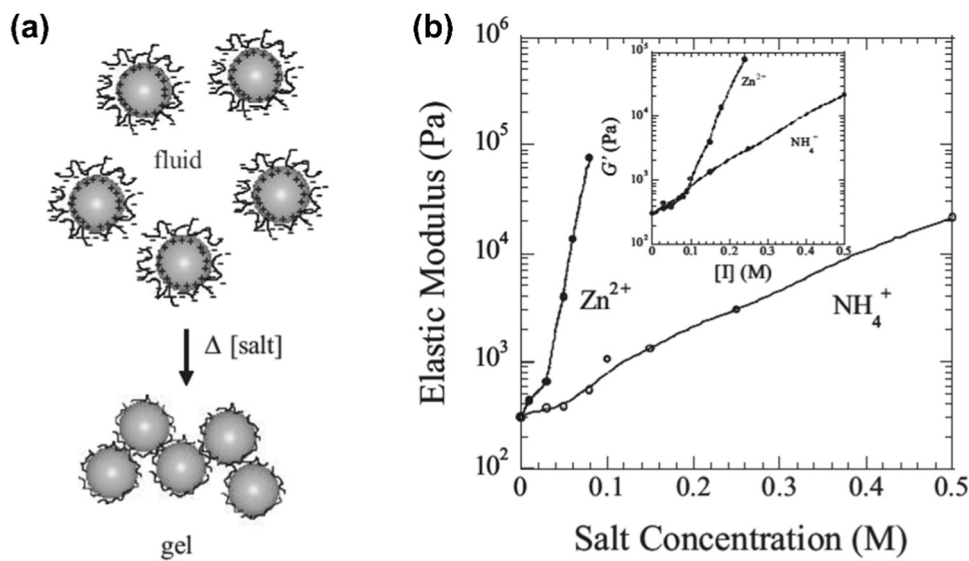


Fig. 4. Effect of the salt solution on the modulus. (a) Schematic illustration showing the transformation from fluid to gel state with the introduction of a salt solution. (b) Variation of the equilibrium elastic modulus for a 50 vol% BT ink, comparing the effects of adding monovalent vs. divalent salts [49]. Reproduced from Ref.: (a-b) [49], with permission from John Wiley and Sons.

2.1.4. Particle size, distribution and morphology

The viscoelastic behaviour of the ink is determined by the physical characteristics of the powder particles, which include their size, size distribution, shape and morphology. These characteristics play a significant role in determining the ink performance.

Several studies suggest that the particle size has a profound effect on the rheological properties of the prepared ink, which in turn affects the final density and the piezoelectric properties of the sintered components [58–61]. In this regard, Renteria *et al.* investigated the effect of various particle sizes of BT (100 nm, 300 nm, 500 nm) on the viscosity and the stress behaviour of the prepared ink using PVA in distilled water [58, 59]. Finer particles exhibited a greater initial viscosity at low shear rates, which subsequently decreased at high shear rates (Fig. 5(a-b)). This is a typical behaviour of pseudoplastic inks which exhibit shear thinning behaviour. As the size of particles decreases, there is an increasing total surface area of the particles that are dispersed and a corresponding reduction in the distance between the particles [62]. Reducing the inter-particle distance leads to an increase in both the frequency of particle contacts and the intensity of particle-particle interactions (mainly Van der Walls forces), resulting in high viscosity and yield stress [63]. At lower shear rates, ceramic particles in the ink have more opportunity to interact and create networks or structures within the solvent with other additives, obstructing the flow and thereby increasing viscosity. However, at higher shear rates, the interactions between the particles and the solvent or additives are disrupted, thereby reducing the viscosity. Conversely, the stress required to make the ink flow also decreases at higher shear. The viscosity difference between small and large particles is diminished at higher shear rates as particles are favourably rearranged with respect to the flow direction.

In addition to the particle size, particle size distribution (PSD) also plays an important role in dictating the rheological behaviour. For an ink formulation, finer powders are more favourable due to their enhanced sinterability. Conversely, coarser particles offer improved flowability but are more susceptible to sedimentation, which can result in unstable inks. Most of the researchers prefer having a narrow size or unimodal distribution of the ceramic particles as it ensures a uniform and consistent interaction with the solvent. On the other hand, bimodal distribution ensures good packing of the powder particles in the ink, as depicted in Fig. 5(c). Recent evidence suggests that using bimodal distribution of powders (replacing 100 nm by 400 nm of BT) helps in reducing the viscosity and the yield stress of the suspension, provided

the volume content of the ceramic particles is kept constant (Fig. 5(d)) [61]. So, when the fine particles are replaced by the coarser ones, the inter-particle distance increases. As a result, there is more space for the finer particles to move around freely [64]. It is widely accepted that the maximum packing fraction of solids increase with increasing polydispersity [65]. In this context, some researchers have intentionally used bismuth molybdate ($Bi_2Mo_2O_9$) powders with a multi-modal particle size distribution [60].

Ceramic particles of various morphologies, such as sphere-like and platelet-like particles have been successfully used in preparing a printable ink [42]. In general, spherical particles are reported to exhibit greater flowability due to decreased inter-particle interactions and friction when flowing across each other. In contrast, platelet-like particles possess larger ellipsoids of rotation in contrast to spherical particles at a given constant volume, leading to increased inter-particle interactions [63,67,68]. Furthermore, these highly anisotropic particles tend to interlock owing to their irregular edges, thereby leading to agglomeration and high viscosity even at low solid loadings [67]. However, if the applied shear stress is capable of aligning the platelets in a single direction, the viscosity drops. Furthermore, using anisotropic templates leads to templated grain growth after sintering, which is reported to provide high piezoelectric properties along the growth direction.

Walton *et al.* studied the effect of the addition of BT (5 – 40 μm) platelets to a lead-based piezoceramic ink ($d_{50} = 0.28 \mu\text{m}$) [52]. It was discovered that, on adding the platelets, the modulus decreased and was further enhanced by increasing the amount from 0.3 vol% to 1.4 vol%. (Fig. 5(e)) This decrease can be attributed to the incorporation of large particles in a matrix constituted of fine powders. Once the dispersity index of the system changed from mono to poly, the viscosity and the modulus of the ink decreased. The modulus decreased gradually with applied shear stress in the ink containing templates, showing that the transition from solid-like to liquid-like behaviour is progressive throughout the range of applied shear stress. Additionally, the yield stress was almost constant ($\sim 1200 \text{ Pa}$) regardless of the volume fraction of the platelets, which was higher than the yield stress ($\sim 530 \text{ Pa}$) of the ink without the platelets. Anisotropic particles such as in the case of platelets tends to have particular directions in which they can align more easily when subjected to a shear stress, in contrast to the spherical particles which lack directionality. As a result, the presence of platelets increases the amount of stress required to overcome their resistance in

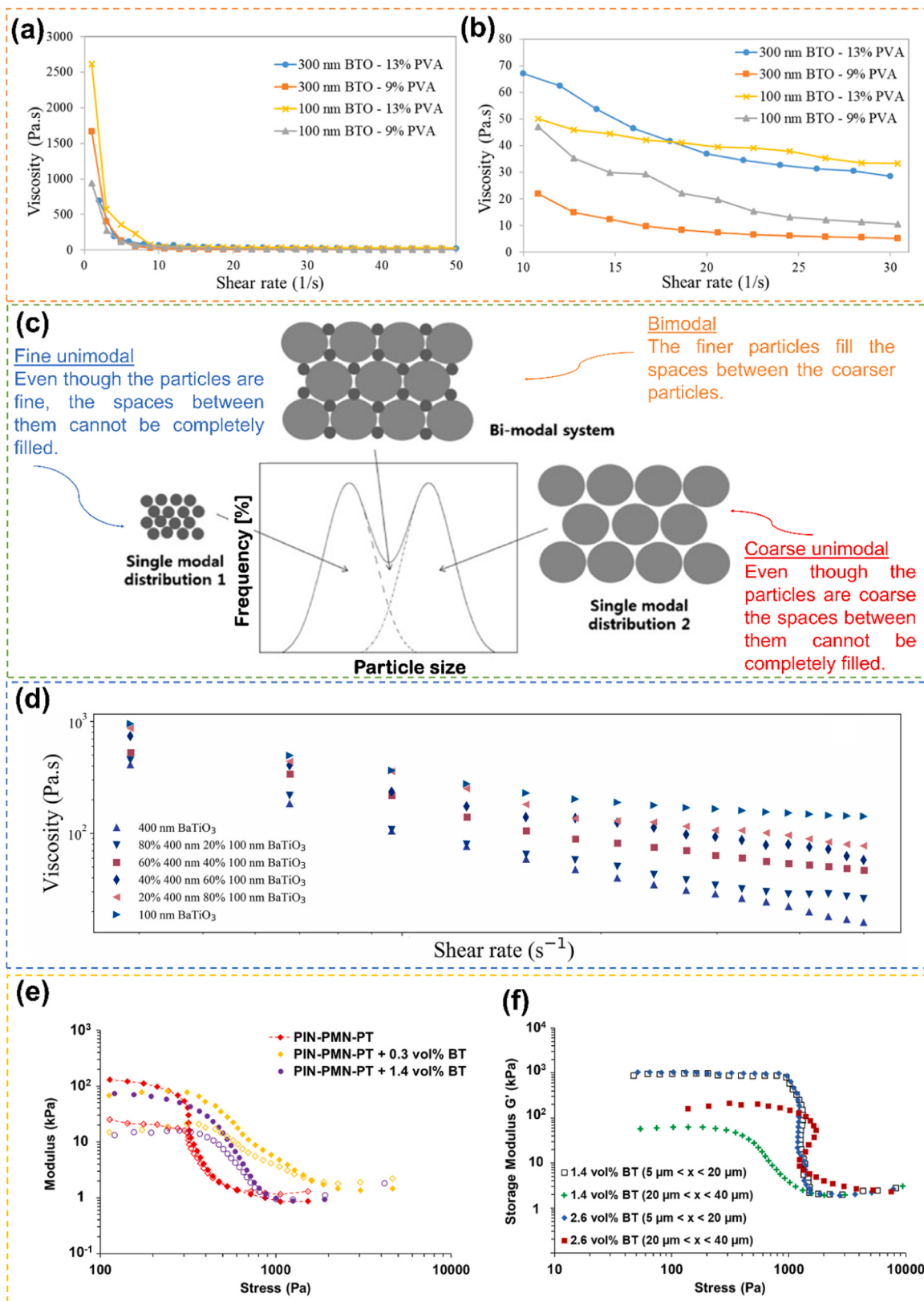


Fig. 5. Impact of particle size, shape and distribution on the rheological behavior. (a-b) Evolution of the viscosity as a function of particle size and binder content for BT inks [59]. (c) Schematic depiction of particle arrangements in unimodal and bimodal particle size distributions [66]. (d) Viscosity as a function of shear rate for monodispersed slurries and bimodal particle distributions with different BT particle size mixing ratios [61]. (e) Storage modulus (solid markers) and loss modulus (open markers) as a function of applied stress for 28 vol% PIN-PMN-PT ink at pH 5, comparing compositions with 0.3 vol% and 1.4 vol% of 2 – 40 μm anisotropic BT platelet particles [52]. (f) Storage modulus vs. applied stress for 28 vol% PIN-PMN-PT ink at pH 5 with varying amount and size fractions of BT platelets [52]. Reproduced from Ref.: (a-b) [59], with permission from IOP publishing. (c) [66], and (d) [61], with permission from Elsevier. (e-f) [52], with permission from John Wiley and Sons.

changing from a random orientation to a particular direction. This is the reason for the presence of a gradual decrease in the modulus as well as increased yield stress in case of an ink which contains platelets. While the volume fraction of the platelets remained constant (1.4 vol%), altering the size of the platelets from small ($5 - 20 \mu\text{m}$) to large ($20 - 40 \mu\text{m}$) resulted in a significant reduction in modulus and a slight increase in yield stress (Fig. 5(f)).

2.1.5. Effect of ceramic loading, binder, coagulant/dispersant concentration

Formulating an ink with high solid loadings ($> 50 \text{ vol\%}$ or 80 wt\% , please refer to Table 2) that display pseudoplastic and viscoelastic behaviour with a low concentration of additives is one of the main challenges in robocasting. The DIW technique is best suited for inks that have extremely high solid loadings for reasons such as high green

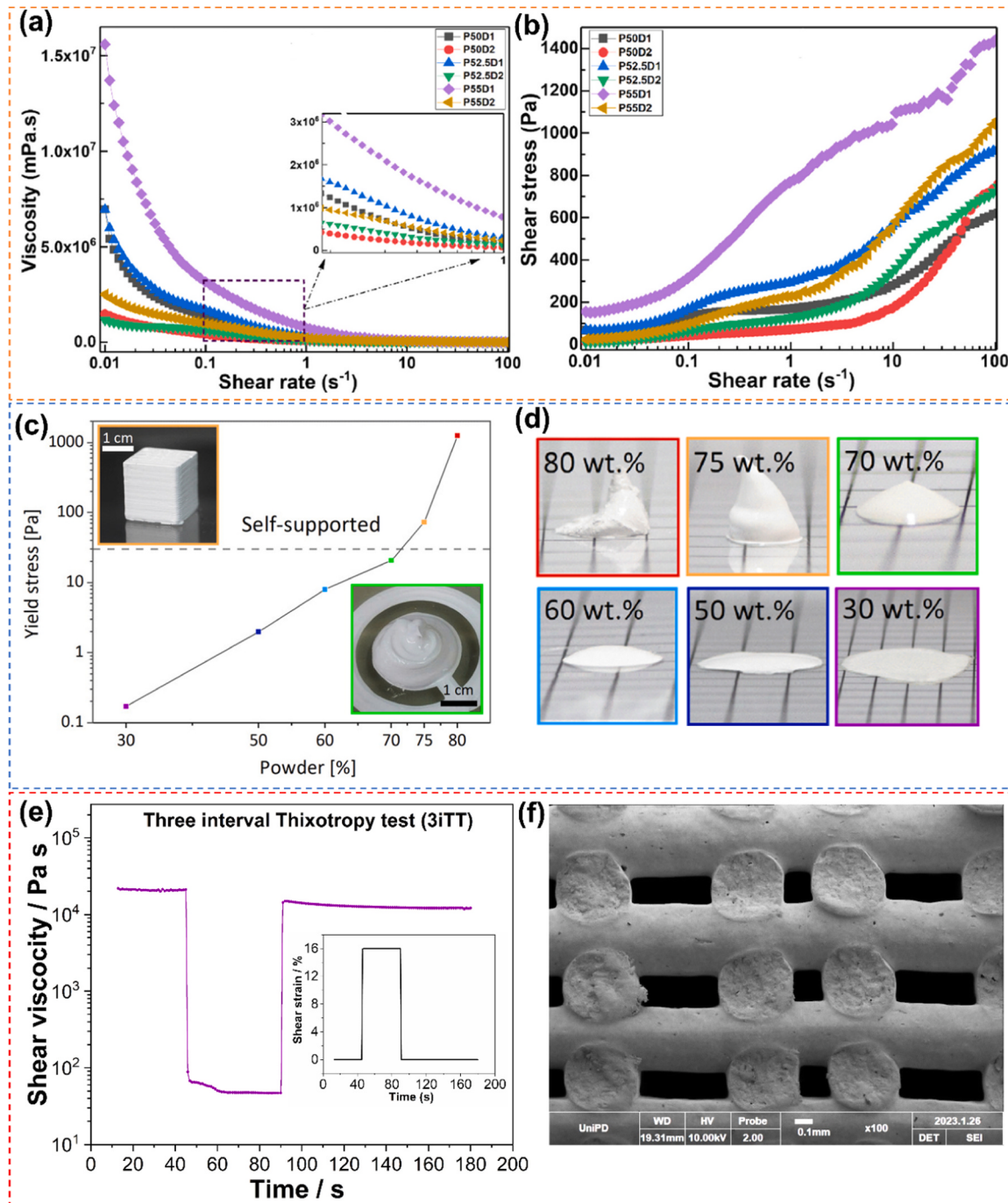


Fig. 6. Effect of ceramic loading on rheological properties and shape retention ability. (a) Viscosity, and (b) Shear stress vs. shear rate for PZT inks with varying solid loadings and dispersant concentrations [74]. (c) Yield stress of BT inks with different solid loadings, with insets illustrating the typical yield behaviour of printed objects using inks containing 70 wt% (lower inset) and 75 wt% (upper inset) ceramic particles [78]. (d) Photographs of various ink formulations shown in (c) exhibiting the shape retention capacity. The images correspond to the graph points in (c), with matching border colours on the pictures for easy reference [78]. (e) The three-interval thixotropy test (3iTT) for measuring the time-dependent recovery of viscosity. The inset depicts the change in shear strain over time [79]. (f) SEM image of the fracture surface of the sample, fabricated using the ink characterized by the 3iTT test shown in (e), highlighting suspended struts within the printed porous lattice [79].

Reproduced from Ref.: (a-b) [74], with permission from Elsevier. (c-d) [78], and (e-f) [79], with permission from John Wiley and Sons.

density of the printed component, minimal shrinkage/warping during the drying process, excellent mechanical properties, and high density following high-temperature sintering process.

Numerous studies have been conducted to study the impact of solid loadings on the rheological characteristics of an ink [52,69–75]. It is widely acknowledged that an increasing solid loading leads to an increasing viscosity, yield stress, flow stress and the modulus of the ink due to more inter-particle interaction. Fig. 6(a-b) depicts the variation of viscosity and shear stress with shear rate. This is a typical example of shear-thinning behaviour, where the viscosity of the material decreases as the shear rate increases, resulting in an increased shear stress. Often the flow curves are fitted according to the Herschel-Bulkley model with the following equation [76]:

$$\sigma = \sigma_y + k\gamma^n \quad (3)$$

where σ is the shear stress (Pa), σ_y is the yield stress of the ink, k is the consistency index, n is the flow index and γ is the applied shear rate (s^{-1}) on the ink. The most important feature to observe is that the ink should exhibit shear-thinning behaviour (when $0 < n < 1$), unlike shear-thickening ($n > 1$) where the viscosity increases with shear rate, making it difficult to extrude through a nozzle. Such shear thickening behaviour has been reported while preparing BCZT ink (44 vol%) and hybrid sol-gel BT ink (40 vol%) [51,73]. This is due to a non-optimal powder dispersion or enhanced powder agglomeration with high solid loading. It is worth noting that the viscosity of the ink can also be influenced by the ageing process, mostly due to the spatial redistribution of the solvent in the ceramic paste [77].

Rosental *et al.* studied the rheological properties with varying amount of BT particles (30–80 wt%) [78]. The authors reported that with high loadings (> 75 wt%), the ink was not extrudable even with a nozzle diameter of 1.5 mm, as validated by the sharp increasing yield stress value showed in Fig. 6(c) [78]. Even though the inks with low solid loadings were extrudable, this did not guarantee that the printed parts were able to retain its shape (Fig. 6(d)). This leads to an important conclusion: *All printable inks are extrudable but not all extrudable inks are printable*. The ability of an extruded filament to retain its shape after the printing process is dictated by the yield stress, storage modulus and the elastic recovery of the ink, which depends on the solid loading.

It is important to note that the recovery time also determines the shape retention, space filling and the roughness of the external surfaces. In this context, Rowland *et al.* studied the effect of different solid loadings on the ink flowability behaviour [71]. Because of the lower water content in high solid loading ink, the ink dried up quickly indicating a short recovery time, leading to distinct noticeable interfaces as observed by optical microscope. On the other hand, an ink with low solid content had a better flowability owing to the slumping effect, leading to a better surface finish without any noticeable interfaces. Similarly, Walton *et al.* studied the effect of recovery time on the space filling behaviour of an ink with BT platelets [52]. The authors reported that the ink with the quick recovery time was not able to fill the space completely, thereby leaving behind residual porosity. Conversely, the ink with larger recovery time was able to completely fill the volume (Fig. 3(b-c)). Indeed, it is clear that the space filling behaviour is related to the recovery time of the ink. Nevertheless, in designs where geometrical porosity or intricate designs or overhanging are desired, the ink with quick recovery time would be better suited. The recovery time of the formulated ink can be easily quantified with the help of a three-interval thixotropy test [41, 79]. The first interval mimics the ink is at rest, the second interval denotes the extrusion process where the viscosity decreases abruptly, and the third interval mimics the condition of the ink after being extruded. One can clearly observe from Fig. 6(e) that almost 90 % of the initial viscosity is achieved within 5 s, ensuring the shape retaining capacity of the overhanging filaments as depicted in Fig. 6(f).

The yield stress defines the resistance to flow of the ink under pressure. The higher the yield stress of the ink, the more pressure is

required for extrusion. In general, the yield stress increases with solid loading [71,78]. An ink with moderate to high yield stress (higher solid loading) is often desired for printing, as it is capable of retaining the structure after extrusion. On the contrary, an ink with low yield stress (lower solid loading) exhibits less resistance to deformation and hence typically deforms/collapses under its own weight before the elastic recovery (Fig. 6(d)). Interestingly, the yield-stress of the ink can also be increased by heating the print bed, which promotes solvent evaporation from the ink and helps the ink to retain the extruded shape [71,80]. Renteria *et al.* intentionally aged the ceramic paste at low temperatures to re-activate the elastic properties of PVA, ensuring enhanced elastic response of the ink after being extruded [58]. A recent study by Li *et al.* reported that by using volatile components such as ethanol in the ink composition leads to rapid drying of the ink, leading to an increasing solid content thus enhancing the modulus/yield stress and the shape retention capacity [72]. Gadea *et al.* also emphasized that the yield stress is strongly related to the solid loading of the sol-gel ink [73]. The hybrid sol-gel BT ink showed relatively consistent yield stress values for solid loadings ranging from 30 to 35 vol%. However, the yield stress increased significantly when the solid loading was increased to 40 vol%.

The yield stress of the ink also plays a significant role in determining the maximum height of the printable object, which is given by [81]:

$$h \approx \frac{\sigma_{yield}}{\rho g} \quad (4)$$

where h is the maximum height of the printed object (mm), σ_{yield} is the yield stress (Pa), g is the acceleration due to gravity ($g = 9.81 \text{ m}\cdot\text{s}^{-2}$) and ρ is the density of the ink ($\text{kg}\cdot\text{m}^{-3}$). One can easily observe from Eq. 4 that inks with higher solid loadings possess higher yield stress, enabling fabrication of large components [73,78].

To facilitate, high solid loadings in the ink, it is necessary to have a homogeneous dispersion of the ceramic powder in the solvent. This is where dispersants play an important role in imparting stability (either through electrostatic, steric or electro-steric mechanisms) to the ceramic particles, which otherwise would tend to flocculate or sediment. Hossain *et al.* carried out a thorough investigation to study the effect of dispersant content on the rheological property of a PZT ink [74]. The storage modulus and yield stress (in addition to the viscosity and the stress) as depicted in Fig. 7(a-b) decreased significantly when dispersant concentration increased from 1 to 2 wt%. This is due to the fact that the polymeric chains of the dispersant adhere more strongly to the surfaces of the particles, which reduces frictional and electrosteric forces and keeps the particles separated, thereby freeing the trapped solvent. However, increasing the dispersant concentration beyond the optimum value negatively affected the rheological properties. The prepared PZT ink slumped due to a comparatively low elastic modulus and yield stress. In addition, excess dispersant creates a disbalance of electroneutrality in the ink [82]. As a result, the attractive forces can dominate over the repulsive forces leading to agglomeration and nozzle clogging during the extrusion. Similar observations were made by Rowlands *et al.* [71]. The authors pointed out that using less than 0.5 wt% of dispersant led to agglomeration and nozzle clogging. A maximum of 1.5 wt% of dispersant was necessary to achieve a stable suspension with homogeneous dispersion of the ceramic particles. However, the dispersant should be carefully selected for a particular binder system. Liu *et al.* reported that *in situ* polymerization of PAA in presence of PVA led to the formation of a gel [83]. In this case, the gelation phenomenon was intensified leading to an increase in viscosity when the PAA concentration exceeded 1.75 wt%.

In contrast to dispersants, coagulants help to achieve the desired rheology by promoting particle agglomeration. Several studies reported the use of polyethylenimine (PEI) as a coagulant [50,51,84]. The addition of PEI is reported to increase the viscosity and storage modulus by orders of magnitude [51]. Furthermore, the linear viscoelastic region (LVR) on adding PEI extends up to higher stress/strain values,

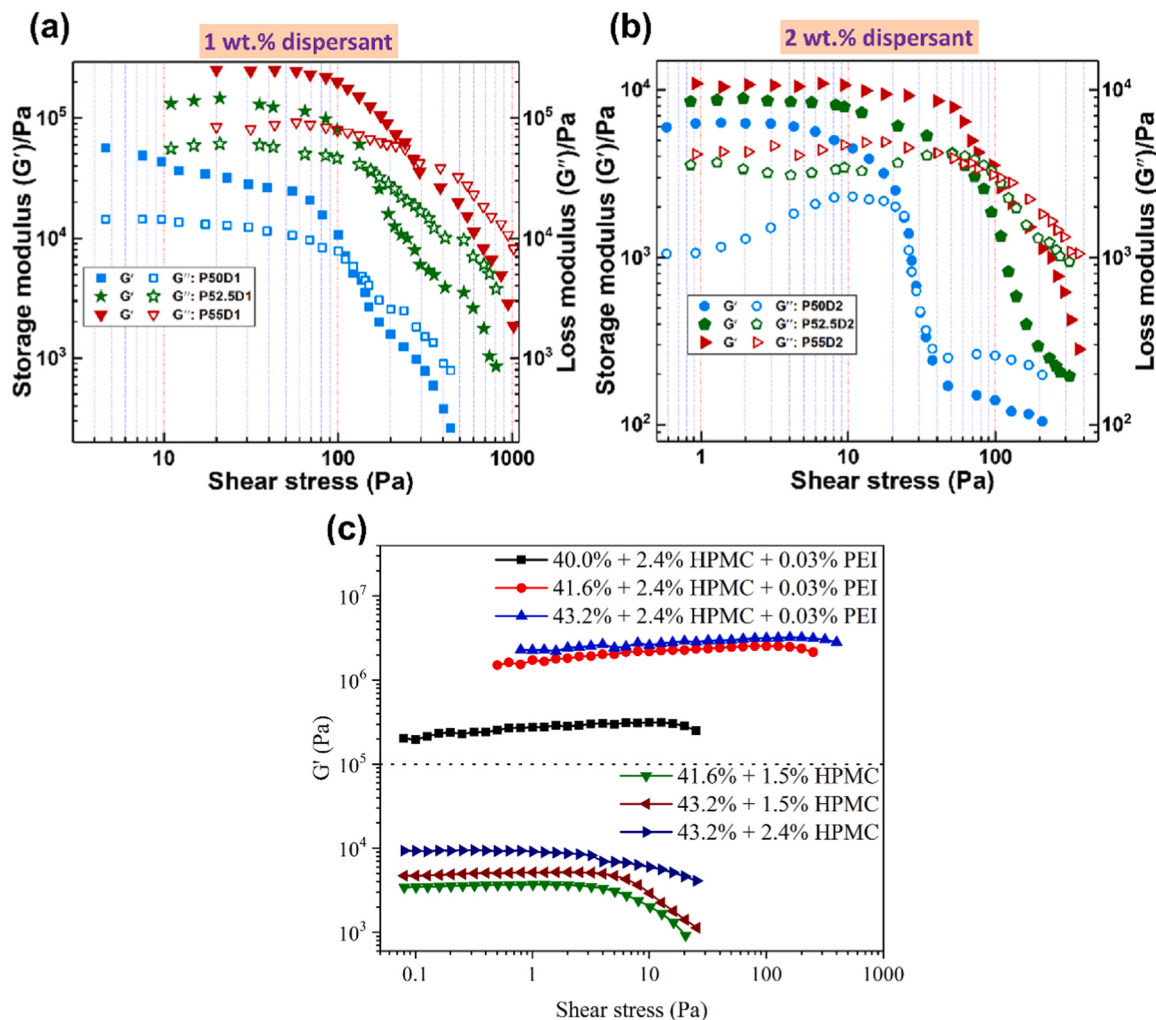


Fig. 7. Effect of dispersant, binder, and coagulant concentration on the rheological behaviour. (a-b) Rheological analysis of PZT inks, showing the relationship between storage modulus (G') and loss modulus (G'') with shear strain for inks with varying dispersant and solid loadings [74]. (c) Variation of elastic modulus (G') with shear stress at different binder (HPMC) and coagulant (PEI) concentrations in BCZT pastes [51].

Reproduced from Ref.: (a-b) [74], with permission from Elsevier. (c) [51], with permission from John Wiley and Sons.

suggesting that the ink possesses higher elastic properties which are necessary for shape retention (Fig. 7(c)). The coagulation phenomenon can be explained by charge neutralization, which occurs when the positively charged secondary and tertiary amino groups in the PEI readily interact with the negatively charged functional groups in the dispersant (Dispex® A40). Nan *et al.* reported that the shape retention capacity of vertical free-standing pillars was enhanced by using 0.032 wt% PEI [84]. Although an excessive amount of PEI (0.068 wt%) improved the ability to form flocs, resulting in an increasing storage modulus, it also led to a reduction in electrostatic interactions between cationic-anionic couples due to multibody effects [84]. Furthermore, the concentration of PEI was maintained below the threshold required for monolayer formation, allowing it to function as a bridging flocculant. Such concentration keeps the PEI molecules more dispersed rather than completely encapsulating the ceramic particles providing more flexibility to interact with multiple particles or creating bridges/connections among the particles. Indeed, the steric hindrance (from the additives) will impose a restriction on the quantity of PEI chains capable of bridging. However, the probability of a PEI molecule forming complexes is expected to increase with the size of the PEI molecule. A similar interaction behaviour of PEI with APA-stabilized BT has also been reported elsewhere [50].

The binder used in formulating the ink also plays an important role in

dictating the adhesion between the layers. In addition, it helps in binding the particles together so that the printed samples have enough strength to be handled during post processing. Liu *et al.* investigated the role of binder (PVA) concentration on the ink viscosity (keeping the solid content fixed at 86.21 wt% of PZT) and found that a binder concentration in the range of 6–12 wt% was suitable for easy extrusion and subsequent shape retention [85]. The viscosity was also reported to increase with the PVA concentration. As the amount of PVA increases, the hydrogen bonding among the PVA chains increases correspondingly, leading to an increasing viscosity. The ink with the highest amount of binder exhibited the least dimensional deviation. This is in good agreement with another study where PVA of 9 wt% and 13 wt% was successfully used in preparing BT inks [59]. Similar variation in the viscosity was also reported for BCZT inks prepared with different contents of hydroxypropyl methylcellulose (HPMC) binder [51]. Kim *et al.* reported phase separation and undesired flow rates during the printing process when the binder (PVDF) to solvent ratio (DMF) was maintained at 1:14 due to low viscosity of the paste on using excessive DMF [86]. On further increasing the ratio to 1:8.8, an ink with better rheology, controlled flow-rate and shape retention was achieved.

2.1.6. Novel ink formulations: capillary suspension and sol-gel

Significant progress has been made in the field of DIW, particularly

with the introduction of unconventional ink formulations that differ from the traditional compositions. Some of these innovative formulations employ capillary and sol-gel based suspensions, offering a new perspective in the field of robocasting.

Unlike colloidal suspensions, where particle stability is determined by electrostatic repulsion or steric hindrance, the stability of particles in capillary suspensions (CapS) is maintained by the capillary forces arising by the addition of an immiscible secondary phase in the bulk phase [87]. Using CapS of BT, researchers in Germany successfully managed to fabricate log-pile structures with 150 µm nozzle diameter [88]. For the preparation of such inks, first a mixture of low viscosity paraffin oil, mineral spirits and stearin wax was heated up to 70°C with constant stirring and then homogenized using a high-speed mixer (2400 rpm). This constituted the bulk phase of the CapS ink. Subsequently, the addition of the secondary phase, i.e. aqueous sucrose solution led to the formation of capillary bridges between the particles with a coherent particle network spanning in the bulk phase. These capillary bridges are known to exist in two forms: pendular bridges, characterized by a contact angle $\theta_{SB} < 90^\circ$ and capillary bridges, characterized by a contact angle $\theta_{SB} > 90^\circ$. The contact angle θ_{SB} is defined as the angle between the secondary phase and the ceramic particles, when surrounded by the bulk phase [89]. In this case, θ_{SB} was calculated to be $31.6^\circ \pm 5.4^\circ$, which implies that the secondary phase was able to wet the ceramic particles, resulting in a stable suspension without any phase-separation. The secondary phase is believed to induce the transition from a fluid (low viscosity) to a highly elastic behaviour, necessary for shape retention. These suspensions are specifically designed for the fabrication of microstructurally porous ceramics. As a result, the ceramic loading was limited to only 31 vol%.

A recent study reported the use of a hybrid sol-gel ink containing BT particles [73]. The ink was prepared by mixing titanium isopropoxide (TTIP) and N-methyl diethanolamine (MDEA) in an argon-filled bottle and subsequently water and glycerol were added in drops. Finally, barium oxide (BaO) was added in stoichiometric concentrations to obtain a gel. In order to maintain the stoichiometry (Ba:Ti = 1:1), it was possible to only have a solid loading of 8 vol%. Such an ink is not suitable for robocasting as it lacks yield stress or shear thinning behaviour. Subsequently, commercial BT powder was added to the ink to increase the solid loading to 30 – 40 vol% and achieve suitable rheological parameters for printing.

One of the advantages of DIW is that it enables the use of a low amount of organic content, and it would be even more beneficial to eliminate the use of organics altogether, since they are one of the most challenging aspects in the thermal treatment (debinding) process. Rosental *et al.* proposed a solution by replacing the organic additives by a sol-gel precursor [78]. The sol-gel precursor was chosen in such a way that it yielded the same composition as the dispersed particles after the heat treatment. This precursor actually acted as a binder for the BT particles and was synthesized via a sol-gel technique using barium acetate and titanium isopropoxide (TTIP) as starting materials, with water and acetic acid as solvents.

2.1.7. Ink formulation steps

To guarantee that the ink formulation for DIW is appropriate for the printing process, it is essential to introduce the processing additives in the correct order, since an incorrect order of addition can significantly impact the quality of the final ink. At first, the dispersant is usually mixed well with the solvent before the ceramic powder is added. Subsequently, the binder, coagulant and other processing additives are added to the system. Although some of the researchers prefer mixing the solvent and all of the processing additives before adding the ceramic powder, in any approach the additives should be added in the following sequence: dispersant → binder → humectant (solvent trap) → coagulant. To guarantee a homogeneous mixing, a mixing step should be performed after each component is added. One of the most efficient methods of mixing is adding the ceramic powder in batches and providing a gap of a

few minutes between two successive mixing steps to avoid heat generation during the mixing process. This can lead to solvent evaporation or initiate some unwanted reaction among the additives. The ink is then transferred to a syringe and then defoamed to remove the entrapped air bubbles.

Instead of adding the dispersant to the solvent, the dispersant can also be mixed well with the powder using an agate mortar or a ball mill before adding it to the solvent. However, while preparing bigger batches, it can be difficult to maintain the homogeneity. Inhomogeneity can also arise due to use of certain additives such as PVA, which does not completely dissolve in deionized water at room temperature. In order to promote dissolution, a certain temperature with constant stirring is required to ensure homogeneous mixing of the binder. It might happen that some of the water evaporates during the process, thereby deviating from the target ink composition. A similar observation was made by Kim *et al.* while mixing PVDF in DMF solvent [86]. After the mixing process, an additional amount of DMF was added to maintain the ratio of the binder to solvent. Using such combination of solvent and binder, Wang *et al.* formulated a stable ink with nanoparticles just by stirring with a glass rod [69].

When formulating the ink composition, it is important to take into account that the amount of added dispersant, binder and coagulant is directly related to the ceramic powder content. The finer the ceramic particles, the more processing additives are required. On the contrary, the humectant (solvent trap) concentration depends on the overall liquid volume. This keeps the ink from drying out too quickly, which otherwise might lead to nozzle clogging.

It might also happen that the prepared ink cannot be completely used immediately after it has been prepared. In this situation, it is necessary to subject the ink to a secondary mixing process to counteract the effects of ageing. Otherwise, an undesirable increase in the viscosity of the ink may occur.

2.1.8. Printing parameters: optimization

The nozzle diameter, printing speed and extrusion pressure plays an important role in determining the quality of the printed component. Understanding the relation between the parameters not only ensures a smooth printing but also higher resolution in the printed component.

The nozzle diameter determines the resolution that is achievable during the printing. As a rule of thumb, the nozzle diameter should be at least 15 times the size of the largest particle size to ensure a smooth flow [40]. Particle agglomerates may compromise this simple rule. The minimum extrusion pressure required by the ink to flow out of the nozzle is governed by the equation [90]:

$$P_{\min} = \frac{4L\sigma_{yield}}{D} \quad (5)$$

where σ_{yield} is the yield stress of the ink, L is the length and D is the diameter of the nozzle. One can easily observe from the Eq. 5 that the value of P_{\min} is strongly affected by the ink rheology (ceramic loading) and the nozzle diameter. It increases with increasing the ceramic loading or by decreasing the nozzle size. Hossain *et al.* carried out a thorough study and reported the variation of the minimum extrusion pressure with the nozzle size [74]. The authors reported that finer nozzle sizes certainly lead to a high resolution, but at the expense of really high extrusion pressure (Fig. 8(a)). On the other hand, using a large nozzle size reduces the printing accuracy. To balance these trade-offs, most of the publications to date, have used nozzle diameters larger than 400 µm (see Table 2), which provides a best compromise between the resolution achievable and the extrusion pressure employed.

Moreover, the extrusion width is also related to the extrusion pressure. It is quite evident from Fig. 8(b), that the strut width increases with increasing the extrusion pressure, while keeping the printing speed constant. Furthermore, as illustrated in Fig. 8(c), the extrusion pressure of the ink with a constant nozzle size is highly dependent on the printing

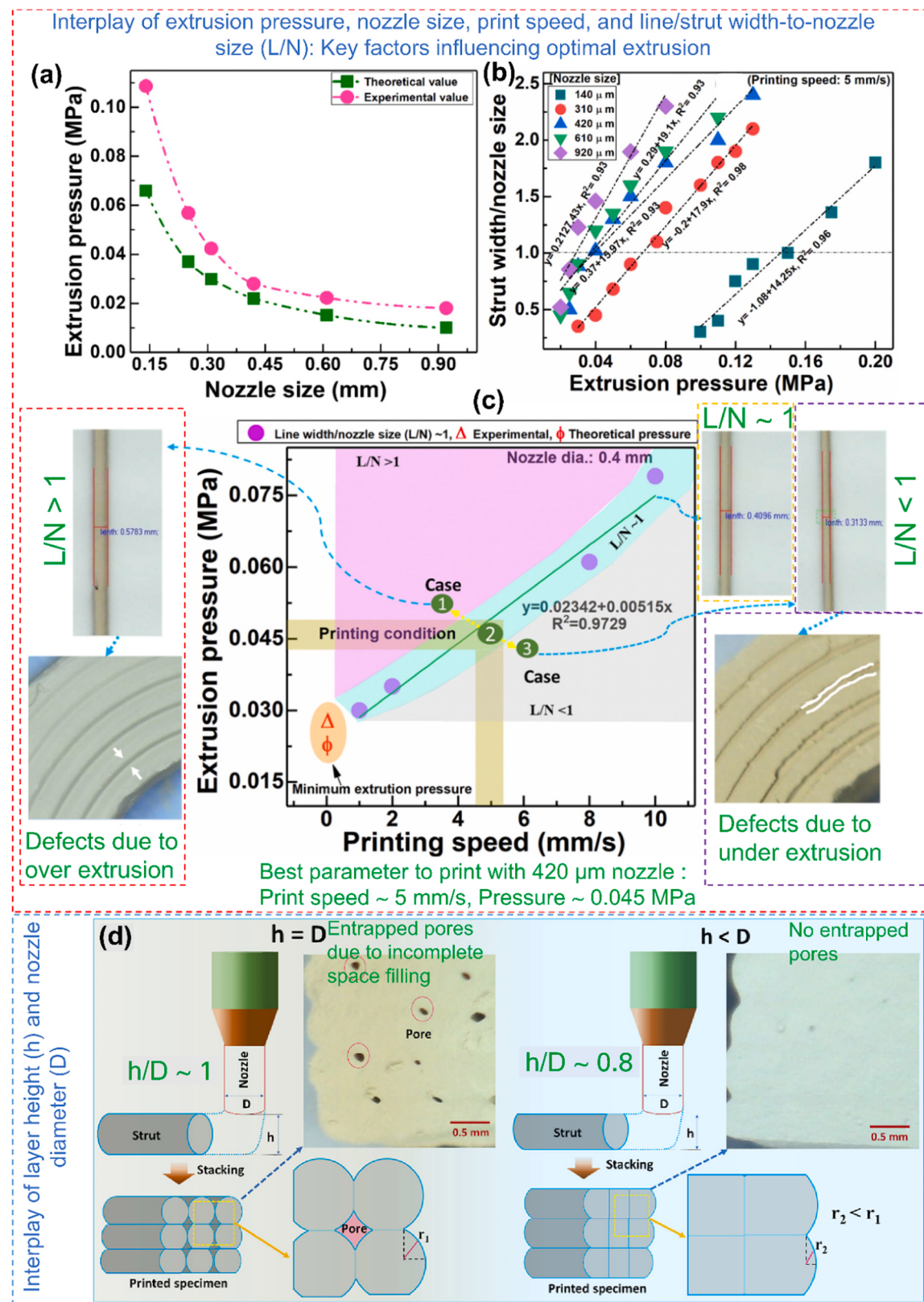


Fig. 8. Factors affecting the print quality. Printing dynamics [74]: (a) Variation in minimum extrusion pressure with nozzle diameter, (b) Effect of nozzle diameter and extrusion pressure on the L (line or strut width) / N (nozzle size) ratio, (c) Extrusion pressure as a function of printing speed for a constant strut width. The images (on the left and right) depict the possible defects that could arise due to under and over extrusion, (d) Factors contributing to inter-strut void formation and strategy for elimination of such entrapped void. This overall analysis was carried out with PZT inks with a solid content of 52.5 vol%.

Reproduced from Ref.: (a-d) [74], with permission from Elsevier.

speed. This indicates that a higher extrusion pressure is required to maintain a constant ratio between the diameter of the nozzle (D) and the width of the extrusion (L), with increasing printing speed. Ideally, a ratio of 1 ensures a defect-free deposition of the ink. On the contrary, deviations lead to defects, as shown in Fig. 8(c).

In addition, the height of the extrusion or the layer height influences the surface finish and the presence of inter-strut porosity. If the layer height is too low, the nozzle has to traverse through the already deposited layer, which leads to build up of material along the printing direction. On the contrary, higher layer height leads to misalignment and improper stacking of struts. This can lead to residual porosity entrapment. The effect of the layer height (H) on the formation of the inter-strut porosity has been shown in Fig. 8(d).

A lower H/D ratio (where, H is the layer height) is always preferred as it increases the curvature length (r) of the deposited strut, thereby minimizing the probability for generating inter-strut porosity. This defect is most prominent when printing dense structures, such as cylinders or bars. This problem could be minimized by using square nozzles instead of circular ones, which theoretically has the highest possible value of r [70]. However, it was discovered that the inter-strut pores were still present. This was due to the entrapment of oil during the movement of the nozzle in oil bath which prevents the ink from drying up at the nozzle leading to nozzle clogging. At the same time, it ensures a homogeneous drying rate after printing. Therefore, printing dense monoliths in oil is not a suitable option. To mitigate these issues, most of

the authors, have used the layer height as 40 – 80 % of the nozzle diameter during printing (please refer to Table 2). This ensures better precision and minimizes the defects related to porosity entrapment.

The ability of particles with a high aspect ratio (e.g., platelets) to self-align along the extrusion path is a key feature of the direct ink writing process. The benefit of such alignment for piezoelectric ceramics lies is the exploitation of the texture-sensitive properties. The material after texturing exhibits enhanced piezoelectric properties along the oriented direction. Nevertheless, textured piezoelectric ceramics are still in the research and development stage, since it is quite difficult to manufacture piezoelectric platelets in bulk quantity. Walton *et al.* carried out a detailed investigation into the alignment process of BT templates in a PIN-PMN-PT matrix [91]. A unique aspect of this study was the implementation of a customized nozzle that incorporated a baffle wall to generate a lateral shear force in addition to the inherent shear effect of the nozzle (Fig. 9(a)). The authors found that the degree of alignment (measured by lotgering factor, explained more in Section 3.2) depends on the nozzle aspect ratio and the printing rate. An increase in both the factors are required to achieve the desired outcome (Fig. 9(b)). Additionally, the platelets were more aligned on the surface compared to the bulk as depicted in Fig. 9(c). In general, the shear rate experienced by the ink depends on the printing rate, according to [81]:

$$\dot{\gamma} \approx \frac{4S}{\pi r} \quad (6)$$

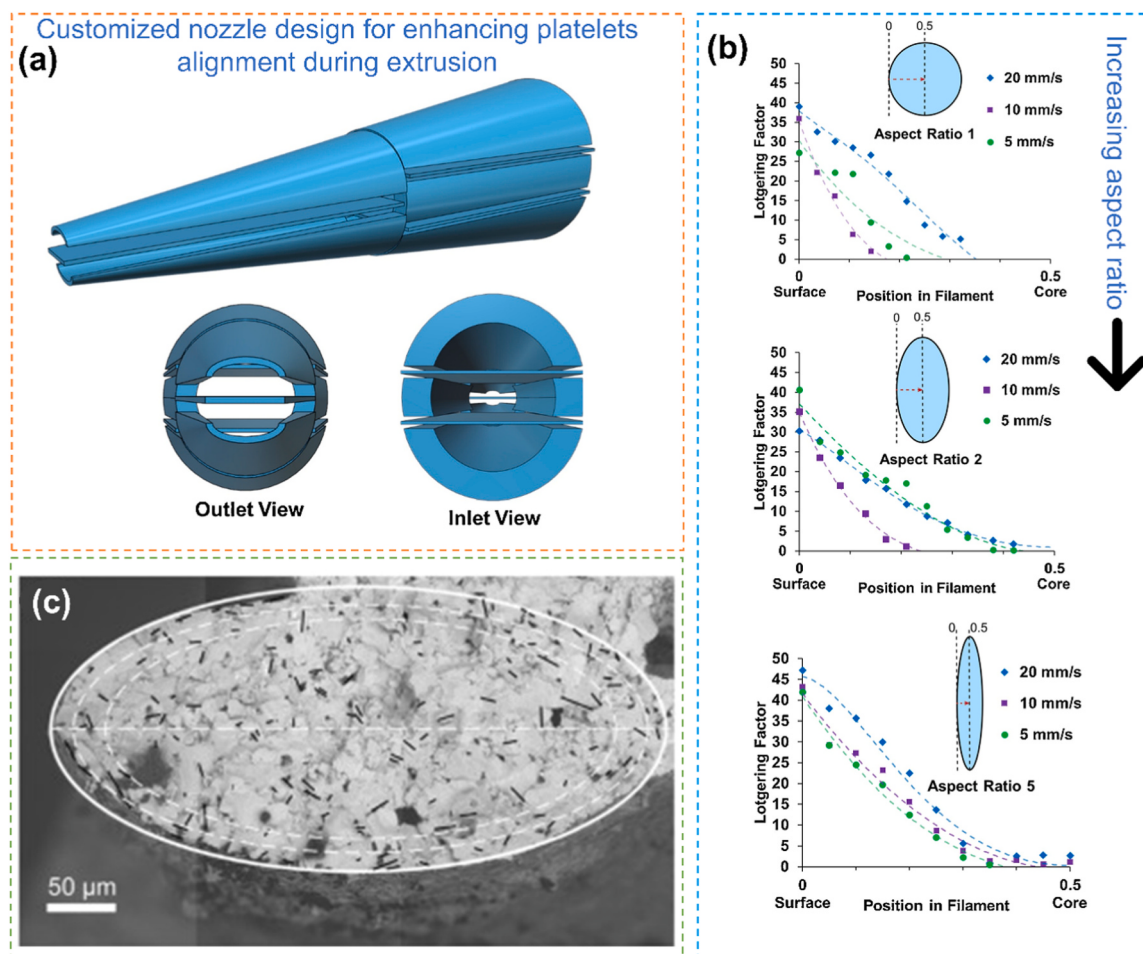


Fig. 9. Impact of nozzle design and printing speed on the alignment of template particles. (a) Schematic of the proposed baffled nozzle for direct writing, featuring an expanded side view, outlet view and inlet view, highlighting the addition of flat baffles within a standard tapered nozzle [91]. (b) Lotgering factor as a function of position (position/diameter) for filaments printed at different printing rates, with comparisons among nozzles of aspect ratios 1, 2, and 5 [91]. (c) The backscattered scanning electron (BSE) image of the sintered filament cross-section shows the alignment of the templates, visible in dark contrast [91]. Reproduced from Ref.: (a-c) [91], with permission from Elsevier.

where $\dot{\gamma}$ denotes the maximum printing shear rate experienced by ink during the extrusion, S denotes the printing speed (mm/s) and r denotes the inner diameter of the nozzle opening (mm). Eq. 6 suggests that using a finer nozzle and higher printing speed will generate more shear stress, thereby enhancing the alignment process more efficiently.

2.2. Fused filament fabrication (FFF) / Fused deposition of ceramics (FDC)

2.2.1. Basics of the technology

In a typical FFF process, the feedstock is composed of ceramic particles embedded in a thermoplastic binder in the form of composite filaments. The binder is usually heated to a molten state and then extruded onto the print bed through a fine nozzle. The slicing software controls the nozzle motion in the X-Y plane, whereas the print bed only moves in the Z direction.

To achieve a high density in the sintered stage, the composite filaments must contain a high loading of ceramic powder. However, this results in increased stiffness, brittleness, and reduced spooling efficiency, which may lead to frequent filament breakages during printing. It is therefore necessary to maintain some degree of flexibility in the filament, as well as low viscosity after melting, to ensure successful printing. In principle, the extrusion mechanism is similar to DIW, which uses a ceramic paste instead of a filament as a feedstock. Two major benefits of using DIW are energy savings, as there is no need to heat the paste for extrusion, and the ability to achieve higher solid loading due to the low organic content. However, the precise control of the rheological behaviour of the paste, which is crucial for the success or failure of the printing process, is not always easy to achieve. In the case of FFF, the ability of the extruded filaments to retain their shape is related to the thermoplastic nature of the binder. It solidifies immediately as it is deposited on the print bed. In such a scenario, FFF offers more shaping flexibility when compared to DIW especially where unsupported or overhangs or structures with numerous retractions are desired. The resolution of the printed components is often dictated by the nozzle diameter which is usually $\geq 400 \mu\text{m}$ (for ceramic-containing filaments, please refer to the Table 3). As a result, this often leads to an uneven surface finish of the components. The green samples can be post-processed to achieve a better surface finish through mechanical processing methods such as milling. In contrast, samples fabricated with DIW are typically more fragile and cannot withstand mechanical processing in the green stage.

The success of the printing process depends entirely on the rheological properties of the feedstock. The following sections will discuss in detail the important factors affecting the filament fabrication process.

2.2.2. Choice of base binder

One of the most important variables that significantly affects the FFF process is the formulation of the binder. In the FFF process, the term binder usually refers to a blend of various polymeric components. This usually consists of a base binder, tackifier, surfactant, wax and plasticizer [99]. Most importantly, the binder and the ceramic powders should be compatible with each other, otherwise it may lead to phase separation during the extrusion process.

In 1998, a team of researchers proposed a four-component binder system for fabricating composite filaments [99]. This binder system, termed ECG9, was extensively used in early studies for fabricating PZT filaments [100–103]. McNulty *et al.* successfully formulated an optimized binder composition with 100 parts of base binder, 20 parts of tackifier, 15 parts of wax and 5 parts of plasticizer to produce PZT filaments [99]. The flexibility of the binder was found to be mostly influenced by the tackifier rather than wax or plasticizer. On the other hand, addition of a tackifier to the base binder resulted in a considerable rise in viscosity and a drastic reduction in the strength. Bandyopadhyay *et al.* reported a similar binder composition to ECG9, but with 6

components [104].

In recent years, several commercial thermoplastic polymers such as acrylonitrile butadiene styrene (ABS), polyvinylidene fluoride (PVDF), polyvinyl alcohol (PVA), thermoplastic polyurethane (TPU), polylactic acid (PLA) and polycaprolactone (PCL) have been widely used as a base binder for incorporating piezoceramic powders [105–113]. Indeed, ABS is considered to be one of the most widely used binder matrices for filament fabrication [114]. This binder is characterized by a relatively low glass transition temperature (T_g) and excellent processing properties, that makes it suitable for the extrusion process. In addition, because of its amorphous nature, the shrinkage associated after the printing process is comparatively small, thereby maintaining a tight dimensional accuracy. In addition, PVDF is becoming increasingly recognized in the field of filament production because of its inherent piezoelectric characteristics [108,115]. The inherent nature of this property makes it a perfect option for further enhancing the properties of the 3D printed composite by using ceramic fillers such as BT (in this case, without sintering the filament after printing). Considering environmental concerns, there has been a recent trend towards the use of biodegradable polymers; PCL stands out to be a better choice concerning environmental challenges [111,113].

Researchers have more recently reported the use of ethyl vinyl acetate copolymer (EVA) as the backbone polymer for fabricating BT and PZT filaments [116,117]. This binder was modified slightly to replace with paraffin wax [118]. The use of a dual-binder system has gradually become important, as the low molecular weight of paraffin wax leads to low viscosity at the shaping conditions and the high-temperature backbone polymer provides sufficient green strength after the shaping and during the debinding process. In addition, paraffin wax usually has a lower melting point and decomposition temperature than the backbone polymer. This paves the path for chemically extracting the wax from the thermoplastic blend (better known as chemical debinding) before carrying out the thermal debinding.

2.2.3. Effect of surfactant, plasticizer

The use of a suitable surfactant ensures that the ceramic particles are homogeneously dispersed in the binder matrix. The dispersion is usually accomplished via steric stabilization [119]. Inhomogeneity can lead to drastic changes in the rheological properties, resulting in a filament unsuitable for the FFF process.

McNulty *et al.* studied the adsorption behaviour of different surfactants, such as oleyl alcohol, stearyl alcohol, oleic acid and stearic acid on PZT-5H powder [120]. It was observed that under similar experimental conditions, adsorption of stearic acid was found to be highest with a value of 8.14 mg/m^2 . While a small quantity of stearyl alcohol (0.811 mg/m^2) was adsorbed, the other surfactants did not adhere to the powder at all. This could be attributed to the limited solubility of the surfactant in toluene, which was used as a milling medium in this study. At similar concentrations of surfactants, stearic acid and stearyl alcohol reached the saturation point and started precipitating. These precipitates easily adsorb onto the powder surface due to electrostatic interactions. In contrast, oleyl alcohol and oleic acid do not reach the saturation point, therefore tend to remain in solution. Moreover, the presence of the COOH group enhances the functionality (better hydrogen-bonding and multiple bonding sites) of the stearic acid in comparison to the OH group in stearyl acid. This is the reason for preferential adsorption of stearic acid over stearyl alcohol. The adsorption process was found to approach saturation when the concentration of stearic acid in toluene reached 30 g/L . Allahverdi *et al.* reported that stearic acid outperforms all other surfactants used for bismuth titanate ($\text{Bi}_4\text{Ti}_3\text{O}_{12}$) powders and the saturation level was found to be 70 g/L [102]. Due to its superior adsorption capabilities, stearic acid has been widely studied as a surfactant [100,101,103,106,116–118,121–123].

Venkataraman *et al.* observed that the relative viscosity of a PZT-ECG 9 composite decreased on addition of surfactants such as KRTTS and

Table 3

Feedstock preparation and optimized printing parameters for fused filament fabrication.

Feedstock	Particle size and morphology	Binder	Additives	Ceramic loading	Printing parameters				Reference
					Nozzle temperature (°C)	Nozzle size (mm)	Layer height (mm)	Additional information	
PZT		ECG9		55 vol%	165 – 170				[99]
PZT-5H	0.5 – 0.7 µm	ECG9	Stearic acid	52 – 60 vol%	145 – 160	0.355, 0.5	0.2 – 0.25		[121]
PZT-5H PZT	0.5 – 0.7 µm SSA = 2.58 m ² /g	Proprietary binder	Oleyl alcohol, Stearyl alcohol, Oleic acid, Stearic acid	60 vol%	145	0.5			[130]
				55 vol%					[120]
PZT	1.2 µm	ECG9	Stearic acid	52.6 vol%	140	0.254, 0.381, 0.508		Filaments stored in controlled humidity	[100]
PZT		ECG2	Stearic acid	60 vol%		0.508	0.254		[122]
PZT	0.73 µm	ECG9	Stearic acid	52.6 vol%		0.508			[101]
BiTi powder	0.5 – 1 µm	ECG9	Stearic acid, KD3, Solisperse 13940	48 – 50 vol% 5 wt%			0.250		[102]
BiTi platelets									
PZT		ECG9	Stearic acid	52 – 60 vol%	140 – 150	0.25 – 0.50	0.025 – 0.25	Build envelope temperature: 20 – 40 °C	[103]
PZT-5H Spray dried BaTiO ₃	< 3 µm	Proprietary from Strstasys ABS (in acetone)		50 – 55 vol% 0 – 70 wt%	140 – 200 230	0.3		Print area temp: 30 °C – 40 °C Print bed: 110 °C	[104]
BaTiO ₃		PVDF (in DMF)		3 – 15 wt%					[108]
BaTiO ₃	Micro-particles	ABS (in acetone)	Octyl gallate, Dibutyl phthalate	32.7 – 33.2 vol%	210 – 225		0.1, 0.2		[105]
PZT	d ₅₀ = 1.1 µm	EVA, Paraffin wax	Stearic acid	60 vol%					[118]
BaTiO ₃	2 µm	EVA	Stearic acid	52 vol% 49 vol%	150 – 180	0.8	0.2	Print bed: 60 °C	[131]
PZT	2.77 µm								
BaTiO ₃	2 µm	EVA	Stearic acid	52 vol% 49 vol%	170	0.8	0.25	Print bed: 60 °C	[116]
PZT	2.77 µm								
BaTiO ₃	3 µm	ABS	Stearic acid	10 – 50 vol%	230	0.3		Print bed: 110 °C	[106]
PZT	0.73 µm	ECG9	Stearic acid (in toluene)	52.6 vol%				Filaments stored at 50 % R.H	[129]
PZT	1.2 µm	ECG9	Stearic acid, KRTTS (both in toluene)	0 – 60 vol%					[124]
SrTiO ₃	500 nm, spherical	ABS		67.89 wt%	240	0.4	0.1 – 0.3	Print bed: 110 °C, Speed: 80 mm/s	[107]
PZT	50 µm spherical granules crushed	Vestoplast V2103, Vestowax SH112, Indopol H-1900, Escorez 1304	Stearic acid (in toluene)	60 vol%	160	0.5, 1.0, 1.2		Speed: 10 – 100 mm/s	[123]
BaSrTiO ₃	APS < 0.5 µm	ABS (in acetone)		0 – 50.27 wt %	250	0.55	0.1	Print speed: 40 mm/s, Print bed: 100 °C	[126]
PZT	500 nm, spherical	TPU/carbon black		30 vol%	230	0.6	0.2	Speed: 20 mm/s, Filament dried at 60 °C for 1 day	[109]
BaTiO ₃	< 2 µm	PCL (in dichloromethane)		25 vol%, 45 vol%, 65 vol %	130	0.4	0.2	Print bed: 30 °C, Speed: 30 mm/s	[111]
BaTiO ₃ , CaTiO ₃ , Ba _{0.64} Sr _{0.36} TiO ₃	< 3 µm	ABS, PP		30 vol%		0.4	0.1		[132]
BaTiO ₃		PLA		17.5 vol%					[110]
BaTiO ₃ , SrTiO ₃ , Ba _{0.67} Sr _{0.33} TiO ₃	< 800 nm	ABS (in acetone)	Dibutyl phthalateoctyl gallate	15 – 30 vol%					[112]
BaTiO ₃	d ₅₀ ~ 2 µm	PVA, PCL		24 – 54.5 vol %	210 – 230	0.3, 0.4	0.2	Speed: 10 mm/s, Filament dried at 60 °C before use	[113]

(continued on next page)

Table 3 (continued)

Feedstock	Particle size and morphology	Binder	Additives	Ceramic loading	Printing parameters				Reference
					Nozzle temperature (°C)	Nozzle size (mm)	Layer height (mm)	Additional information	
PZT 5 H		Multi component binder		50 – 55 vol%	150 – 200	0.3		Build envelope temperature: 38 – 42 °C	[133]
BaTiO ₃ , CNT	700 nm	PVDF (in DMF)		6 – 75 wt%	220	0.34		Print speed: 5 mm/s, Print bed: 120 °C	[115]

stearic acid [124]. However, the one treated with stearic acid displayed the lowest relative viscosity. The mechanism behind the decrease in the viscosity was understood with the help of the Krieger-Dougherty model. The model is best described with the equation [125]:

$$\eta_r = \left(1 - \frac{\phi}{\phi_m}\right)^{-K_E \phi_m} \quad (7)$$

where, η_r is the relative viscosity, ϕ is the solid loading, ϕ_m is an empirical constant known as the maximum packing factor and K_E is an empirical constant called the generalized Einstein coefficient. One can observe from Eq. 7, that the viscosity decreases with increasing packing efficiency. The packing efficiency can be enhanced by the addition of surfactants by decreasing the inter-particle interactions. The greater value of $\phi_m = 0.73$ for the treated group, as opposed to 0.66 for the

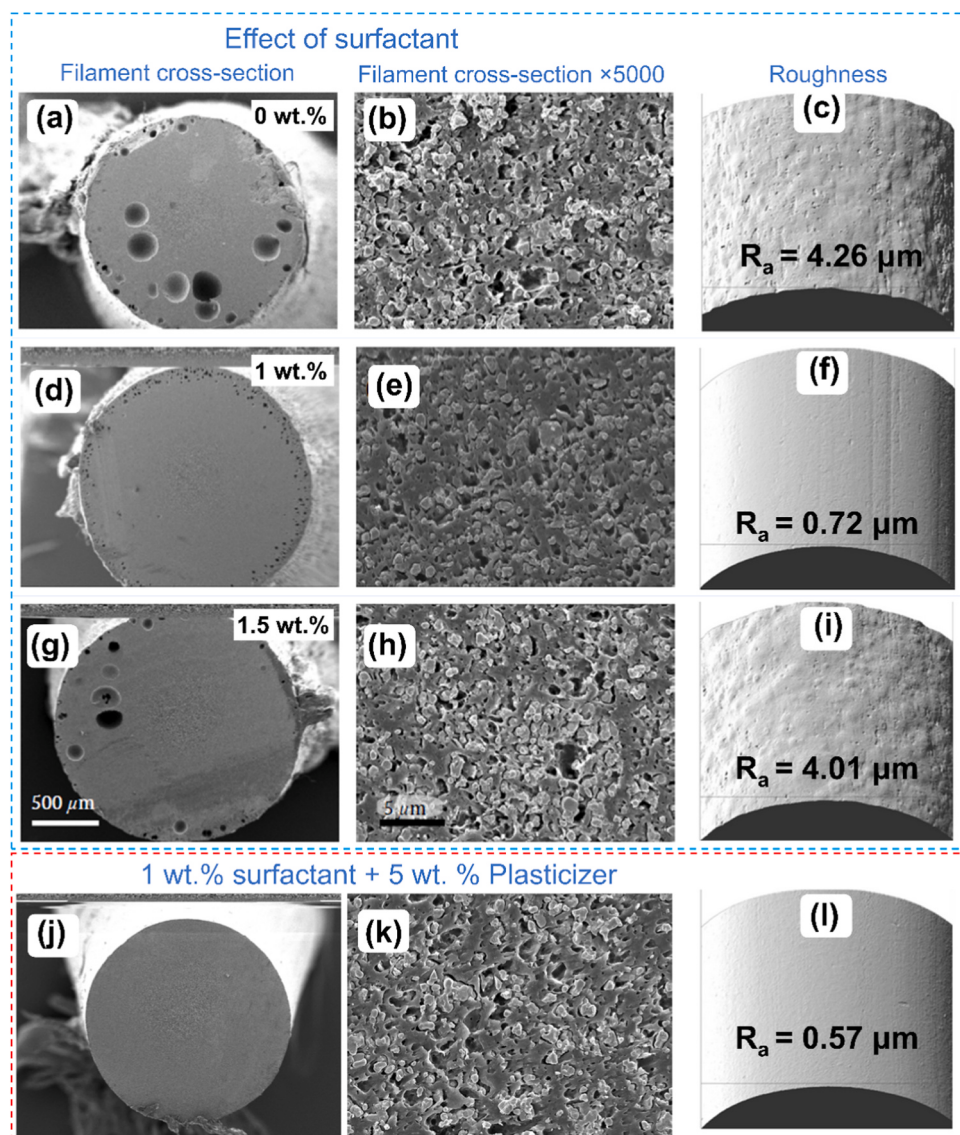


Fig. 10. Effect of the surfactant and plasticizer on the extruded filament. Overview scanning electron microscopy (SEM) images of the cross-section of 30 vol% BT/acrylonitrile butadiene styrene (ABS) filaments with different amounts of surfactant (octyl gallate) [105]: (a-c) 0 wt%, (d-f) 1.0 wt%, (g-i) 1.5 wt%, and (j-l) with 1 wt% surfactant + 5 wt% of plasticizer (dibutyl phthalate), along with the corresponding optical images showing surface roughness. (a-l) [105], Open access article distributed under the terms of the Creative Commons CC BY license.

untreated group, provided further evidence of better dispersion and packing. The empirical Einstein constant has a maximum value of 2.5 for equiaxed particles and this value can either increase if the particles are not equiaxed or decrease in case of slippage at the ceramic particle/polymer interface. The powder treated with stearic acid had a K_E value of 1.49 as opposed to a value of 2.5 for the untreated and treated with KRTTS, suggesting slippage at the interface. Although the exact reason behind such phenomenon was not clear, slippage may have resulted from the local presence of stearic acid in the polymer matrix, which may locally lower the viscosity. It also implies that stearic acid has also lubricating properties in addition to dispersing properties.

Wu *et al.* systematically studied the effect of different concentration of surfactant (octyl gallate) and plasticizer (dibutyl phthalate) on the extruded BT filament [105]. The addition of 1 wt% of the surfactant (octyl gallate) resulted in a reduction in porosity, as it enhanced the interaction between the ceramic particles and the polymer matrix (Fig. 10(d-e)). An excessive amount of surfactant results in the reappearance of porosity in the filament, as shown in Fig. 10(g-h), which is similar to the one reported in Fig. 10(a-b) without the use of any surfactant. However, there is still some residual porosity left in the filament even after using the optimized amount of surfactant. The residual porosity and the surface roughness can be further decreased using 5 wt% of plasticizers (dibutyl phthalate), as shown in Fig. 10(j-k). The plasticizer acts as lubricant enhancing the mobility of the polymer chains and occupying the free space. This effect is also realized in the form of decreased extrusion pressure. The coarse texture (or high roughness) of the filaments with insufficient or excess surfactant is a result of the aggregation of the powder, as demonstrated in Fig. 10(c, i) with high R_a values. With sufficient amount of surfactant (1 wt%), the R_a value decreased to 0.72 μm Fig. 10(f). Conversely, the filament with the optimum surfactant (1 wt%) and plasticizer (5 wt%) exhibited a smooth surface with a further decrease in the R_a value to 0.57 μm as depicted in Fig. 10(l). In addition, the flexibility of the filaments was measured by a two-point filament test device. The curvature of the bending filaments was noted just before the fracture, which revealed that the filament with 1 wt% of surfactant and 5 wt% of plasticizers had similar curvature of radius as the pure ABS filament (4.5 cm) before failure. The lower the curvature value at the fracture, the more flexible is the filament.

In a recent study, Goulas *et al.* reported the impact of not employing surfactant or plasticizer in the filament fabrication process employing $(\text{Ba},\text{Sr})\text{TiO}_3$ (BST) powder [126]. It was found that the printed composite exhibited agglomerated microstructure of the BST powder as shown in Fig. 11, which suggests that the ceramic fillers were not homogeneously distributed in the thermoplastic binder matrix. When submicron solid particles are dispersed into binder matrix without using the surfactant, they often form agglomerates due to strong electrostatic attraction. As a result, the ceramic loading in this experiment was limited to 50.25 wt% (15.26 vol%). Any composition exceeding this limit caused the filament to become brittle and challenging to extrude.

2.2.4. Effect of ceramic loading, flexibility

Usually, a filament with high ceramic loading (> 50 – 55 vol% or > 70 wt%), refer to Table 3) is preferred to minimize the shrinkage, thereby reducing the probability of warping or cracking during the binder burn out process. Nevertheless, increasing the ceramic loading in the filaments induces brittleness (in other words, the compressive or elastic modulus also increases), which in turn causes filament fracture at the gears during the unspooling of the filaments or nozzle clogging during the extrusion.

According to Castles *et al.*, printing filaments with more than 70 wt% (29 vol%) of BT powder was impossible due to their excessive brittleness [127]. It is widely acknowledged that increasing the solid loadings in the filaments increases the viscosity, resulting in the filament being more fragile. Khatri *et al.* carried out a thorough characterization of the filaments with different weight fractions of BT [106]. The torque measurements obtained at the end of the kneading process indicated that the

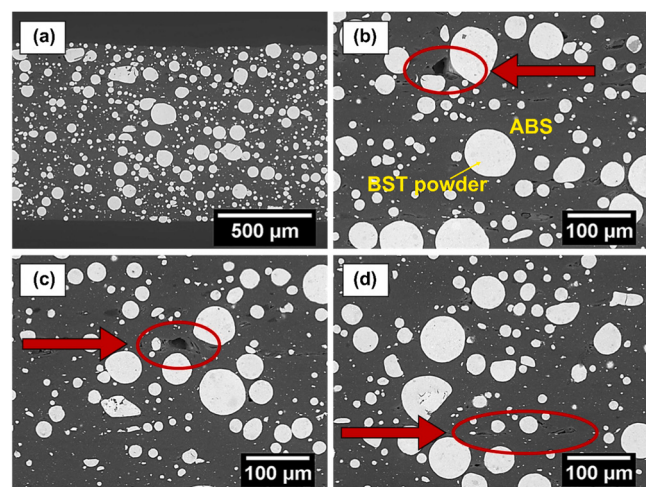


Fig. 11. Consequences of excluding surfactant and plasticizer. (a) Overview, and (b-d) Magnified SEM images of the cross-section of BST/ABS 3D-printed test samples at 50.27 wt% ceramic loadings (15.26 vol%). Arrows indicate defects that adversely affect the dielectric and physical properties of the samples [126].

Reproduced from Ref.: (a-d) [126], with permission from Elsevier.

torque value increased with the ceramic content. However, when the temperature was increased to 210 °C, the torque value dropped, as reported for the filament containing 35 % by volume of the ceramic powder. Since viscosity is a temperature dependent property, it decreases with increasing temperature, resulting in reduced resistance to flow during the kneading process. In addition, the composites up to 35 vol% of BT, exhibited shear-thinning behaviour (Fig. 12(a)). Further increasing the ceramic content to 40 vol% lead to a brittle filament, with filament breakage at the gripping motors. The composite with 45 and 50 vol% of ceramics, exhibited a stick-slip phenomenon (Fig. 12(b)). Consequently, the filaments containing high ceramic loadings (> 40 vol %) were challenging to extrude, resulting in substantial dimensional imperfections in the printed component. In a recent study, authors have reported that a maximum of 80 wt% of BT powder (45.8 vol%) could be incorporated in the thermoplastic matrix for a smooth printing and the shear thinning behaviour became more pronounced (n decreases from ~0.61 to ~0.34) with increase in the ceramic content [113]. The authors also reported an innovative way of measuring the elastic modulus and the maximum stress before buckling in compression mode to simulate similar conditions during FFF printing (Fig. 12(c-d)). The typical force-displacement curves reported in Fig. 12(e) suggest that with increasing ceramic loadings in the filament, the elastic modulus and the maximum stress before buckling increases. However, with lower solid loadings, the filament buckle and then deform plastically. In contrast, filaments with higher solid loadings exhibited a fracture as denoted by a sudden drop in the force values. The fracture behaviour of the filaments is clearly evidenced in Fig. 12(c-d). The filaments exhibited elastic modulus and critical stress before failure in the range of approximately 102 – 556 MPa and 3.5 – 9.6 MPa, respectively, with the highest values recorded for filaments with the highest ceramic loading and the lowest values for those with lower ceramic loading.

2.2.5. Process maps to avoid buckling

In the FFF process, the filament acts as a piston ensuring smooth extrusion during the printing process. This means that the filament should be able to generate and maintain the necessary pressure for facilitating the extrusion process. Failing to do so, results in buckling. The critical stress value required for buckling is denoted by [128]:

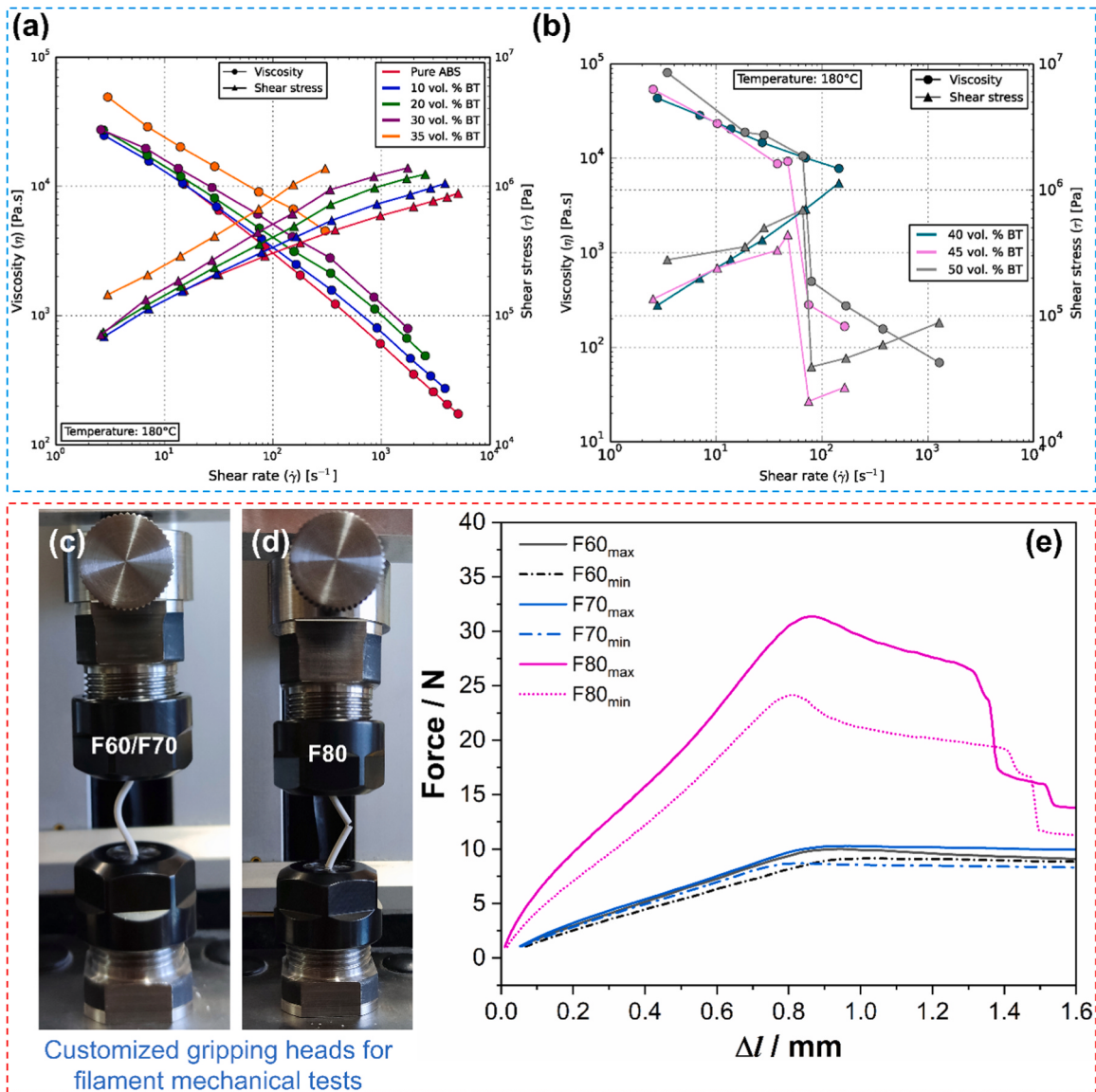


Fig. 12. Effect of the ceramic loading on the rheological and mechanical property of the filament. Rheological analysis of ABS-BT composites with varying solid loadings (a) suitable, and (b) unsuitable for printing. The 45 vol% and 50 vol% samples exhibit stick-slip-like behaviour [106]. Compression test setup for the composite filaments illustrating the buckling/fracture behaviour for filaments with: (c) 60 wt%, and 70 wt% of BT powder denoted as F60 and F70, respectively and (d) 80 wt% of powder, denoted as F80 [113]. (e) Typical force vs. displacement curves for the filaments carried out using the setup show in (c-d), with curves representing the maximum and minimum slopes for each filament type [113].

(a-b) [106], Open access article distributed under the terms of the Creative Commons CC BY license. Reproduced from Ref.: (c-e) [113], with permission from Elsevier.

$$\sigma_{cr} = \frac{\pi^2 E}{4 \left(\frac{L}{R} \right)^2} \quad (8)$$

where σ_{cr} is the critical buckling stress, E is the compressive elastic modulus and L/R is the aspect ratio of the filament above liquefier, where the solid filament is heated and melted into a molten form before being extruded. It is quite evident from Eq. 8 that the critical stress required for buckling is directly proportional to the compressive elastic modulus of the filament. A filament with a higher ceramic loading tends to have a higher elastic modulus, thereby minimizing the risk of buckling. However, there needs to be a balance between the ceramic loading and the modulus, to ensure that the filament is flexible enough to be spooled/de-spooled. The ratio (L/R), also known as slenderness ratio, is a parameter specific to each printer. A printer with a direct drive is preferred over one with a Bowden tube, in order to minimize this ratio.

Venkataraman *et al.* developed a process map to predict conditions that might lead to buckling of the filament [100]. The map relies on two crucial factors: the pressure necessary for extrusion and the compressive elastic modulus of the filament. The pressure drop was found to increase with the flow rate and the aspect ratio of the nozzle. The extrusion process was simulated and the results indicated that the maximum pressure (90 %) drop takes place above the nozzle. This indicates that alterations to the nozzle geometry will have an impact on both the pressure drop and the buckling process. The conditions for buckling was determined by plotting P/E as a function of nozzle geometry and flow rate. In general, buckling should occur if the P/E value is greater than the P_{cr}/E value, as denoted by the shaded region above the horizontal straight line in Fig. 13. The process map suggests that the tendency to buckling increases with increasing flow rate and decreasing the nozzle diameter. Moreover, the aspect ratio of the nozzle plays an important role. One can easily observe that on increasing the L/D ratio from 2 to 5

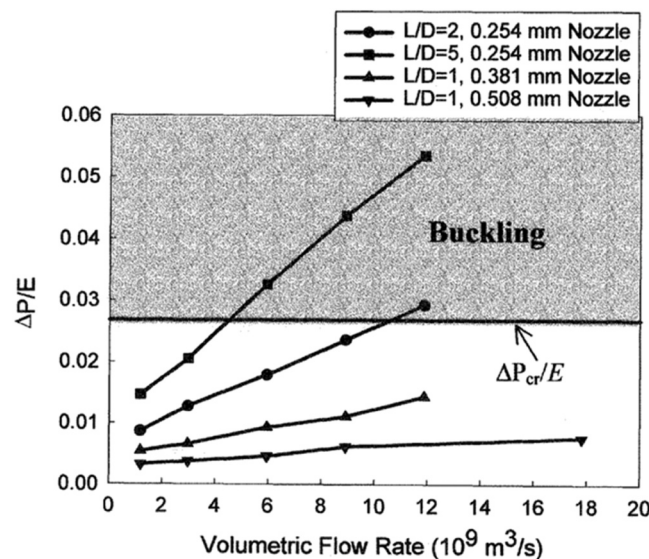


Fig. 13. Process map for predicting buckling in PZT ECG9 filament, illustrating the variation of the dimensionless quantity $\Delta P/E$ with fused deposition ceramic (FDC) nozzle diameter, aspect ratio and volumetric flow rate, measured at 140 °C. The dimensionless quantity represents the ratio of pressure drop (ΔP) to the elastic modulus (E) of the material, both measured in pascals (Pa) [100].

and keeping the nozzle diameter fixed at 0.254 mm, buckling occurs at relatively low volumetric flow rate. It is also clear that the buckling does not occur even at high flow rates with nozzle diameters of 0.508 mm and 0.381 mm. Such findings suggest that printing parameters must be carefully selected to ensure trouble-free printing when using finer nozzle sizes. These predictions have been further confirmed by carrying out independent extrusion measurements. It is important to note that this process map provides only a qualitative analysis, as it does consider the thermal effects or the rate dependence which might also affect the elastic modulus.

Venkataraman et al. proposed a new methodology to assess the filament buckling which was based on the ratio of compressive modulus (E) to the apparent viscosity (η_a) of the extruded filament [101]. The conditions derived for buckling can be written as [101]:

$$\frac{E}{\eta_a} < \frac{8Ql\left(\frac{L}{R}\right)^2}{\pi^3 r^4 k} \quad (9)$$

where Q is volumetric flow rate, R is the filament radius, L is the length between the extrusion mechanism and the printing head and l and r are length and radius of the nozzle respectively. One can easily observe from Eq. 9 that, for a particular printer configuration and flow rate, if the E/η_a value of the filament exceeds a critical threshold, it will buckle. In other words, the ratio has to be maximized to decrease the probability for buckling. It was reported that the critical value of E/η_a to avoid buckling is around $3-5 \times 10^5$ in a shear rate range of $100 - 200 \text{ s}^{-1}$. The authors claimed that this can serve only as a tool for selecting filaments based on the basic mechanical and rheological characterization of the filaments.

2.2.6. Filament production process

The first step in the filament fabrication process is the selection of the suitable binder. Thereafter, comes the powder coating step in which the ceramic particles are coated with the suitable surfactant. Now, there can be two different approaches for extruding the filaments: (i) solvent casting, and (ii) dry mixing.

In solvent casting, first the binder is completely dissolved in a solvent at a certain temperature with constant stirring to ensure homogeneous dispersion. The ceramic powder is then introduced to the binder solution

and mixed well. This solution is now dispersed on a glass substrate/polytetrafluoroethylene (PTFE) plate and heated at a certain temperature to completely remove the solvent. This results into thin sheets of a polymer-ceramic composite, which can be further sliced down to small pieces for easy extrusion with the extruder.

In the dry mixing process, the binder is added to a shear mixer or torque rheometer where it is melted. To this molten binder, the ceramic powder is added in batches. This is basically done to de-agglomerate the powder and ensure a homogeneous mixing. The feedstock is then granulated into small pieces to be used as a feedstock for the final extrusion process. The granulates are fed to the extruder, where the second mixing happens and then extruded into filaments of desired diameter. In case the ceramic powder has not been coated before, the surfactant can also be added during the first extrusion.

It is important to note that, prior to the compounding process, the binders, additives and ceramic powder should be dried. Failure to do so might lead to rough/uneven surface of the extruded filaments due to moisture or residual solvent evaporation during the extrusion process [113]. Castles et al. reported that the composite mixture of ABS and BT particles was left in the oven at 70 °C for a week to ensure the complete removal of acetone, which was used as a solvent to dissolve the binder [127]. Residual acetone, if present, could have produced defects in form of bubbling on the extruded filaments.

It is also important to keep in mind the aging effects after the filament has been fabricated. Venkataraman et al. reported that the filaments tend to become more flexible with time, indicating that the modulus decreases with time. Such a phenomenon is undesirable for the printing process [129]. In addition, some of the most commonly used thermoplastic binders are hygroscopic in nature. In such a scenario, the filaments should be kept in a desiccator to prevent moisture absorption or dried in an oven before using it.

2.2.7. Printing dynamics

There are several important parameters that play a important role in determining the success or failure of the printing job. The printability of the filaments can be easily assessed by examining the external surface of the filaments after it passes through the feeder gears, as depicted in Fig. 14 [113]. In case of a printable filament, regular and distinct gear tooth marks can be observed (Fig. 14(a-b)). On the other hand, the non-printable filament exhibits irregular gear tooth marks with extensive surface grinding (Fig. 14(c-d)).

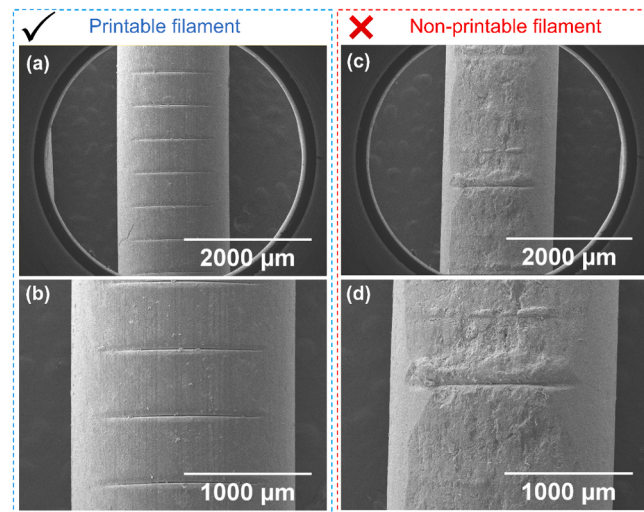


Fig. 14. Overview SEM images highlighting the clear difference between (a-b) a printable and (c-d) a non-printable filament. The images show in (b, d) are magnified version of (a, c) [113].

Reproduced from Ref.: (a-d) [113], with permission from Elsevier.

During the printing process, the nozzle is heated to a certain temperature (usually above the glass transition temperature (T_g) of thermoplastic binder) to provide a shear-thinning behaviour that allows the filament to get deposited on the print bed. Higher nozzle temperatures lead to better bonding between the layers. On the other hand, extremely high temperatures might lead to polymer decomposition. The threshold temperature can be easily assessed by performing a differential scanning calorimetry (DSC) analysis on the composite system.

In this regard, Goulias *et al.* analysed the DSC thermographs of a commercial filament with ABS matrix and strontium titanate (SrTiO_3) as ceramic filler in it [107]. The DSC analysis revealed two T_g at 68 °C and 105 °C and the thermal decomposition temperature at 285 °C. So, in this case the limiting extrusion temperature was 285 °C, beyond which the polymer starts to decompose. Accordingly, the nozzle temperature was chosen to be 240 °C. The print bed temperature is also important when adhesion to the print bed can be an issue. The bed temperature is suggested to be kept above T_g so that it forms a strong foundation for the 3D printed component. In cases where there is a strong affinity between the printed composite and a build plate, a tape can be used on the print bed for easy removal of the sample [116]. On the other hand, adhesive spray can also be used on the print bed to enhance the binding between the extruded filament and the print bed. The build chamber in the FFF printer can be sometimes heated to ensure that no thermal fluctuations would occur during the printing process.

The nozzle diameter determines the resolution of the printed component. A smaller orifice would enable deposition of thinner lines or layers, which can be particularly advantageous when printing intricate designs or small-scale objects. A better compromise between the resolution and the printability is achieved when printed using nozzles $\geq 400 \mu\text{m}$ as reported by several studies (refer to Table 3). However, there is a practical limit which is determined by the viscosity or the ceramic loading in the composite. Umarji *et al.* observed that by reducing the solid loadings from 60 vol% to 52.5 vol%, it was possible to employ a smaller nozzle size of 355 μm instead of 500 μm for fabricating tube actuators [121]. Bhandari *et al.* reported that filaments with lower ceramic content (60 – 70 wt%) could be printed with a 0.3 mm nozzle, although a higher temperature was required compared to using a 0.4 mm nozzle [113]. In contrast, filaments with 80 wt% of ceramic loading could not be extruded due to nozzle clogging. Increasing the nozzle temperature (viscosity decreases with temperature) can be an option which might help in easy extrusion. However, the limiting temperatures have to be kept in mind. As discussed in the Section 2.2.5, the

probability of buckling and nozzle clogging also increases with decreasing nozzle diameter. In order to extrude through a fine nozzle, there has to be a compromise on the ceramic loading.

The thickness of each layer significantly affects the total time and expenses involved in fabricating the printed part. This is because a thicker layer will need less time to finish in contrast to a thin layer. In addition, it also determines the resolution along the z-axis and the aesthetics in terms of smooth or rough surface finishes. Goulias *et al.* discovered that a layer height of 200 μm is optimal for producing dense components with minimal porosity between the printed struts (Fig. 15 (c)), using commercially available filaments based on an ABS matrix containing strontium titanate (SrTiO_3) ceramics of high relative permittivity (ϵ_r) [107]. This is particularly important for dielectric measurements since the functional characteristics are negatively affected by the presence of porosity. The presence of air gaps (Fig. 15(a-b, d-e)) was observed as a consequence of deviations from the optimal layer height (100, 150, 250, 300). To address this issue, it is generally advisable to maintain the layer height between 30 % and 75 % of the nozzle diameter (refer to Table 3). This strategy facilitates a larger contact surface area between the filament and the print bed during extrusion, which enhances adhesion and lowers the likelihood of pore entrapment in subsequent layers.

The layer height is of utmost importance when it comes to aligning platelets for inducing templated grain development. Allahverdi *et al.* studied the degree of texturing using platelets in the fabricated bismuth titanate filament and the printed component, to find out the optimum deposition parameters [102]. The results indicate that platelet alignment on the filament surface was parallel to the direction of extrusion, while platelet orientation within the filament was predominantly random. This is similar to what has been observed during DIW of platelet-based inks (Fig. 9(b-c)). To optimize the alignment of the platelets, a printing layer height of 250 μm was used. Depositing thin layers instead of thick layers results in the application of a significantly higher shear stress acting on the platelets, forcing them to align along the printing direction.

It is important to note that circularity and filament diameter play a crucial role in the printing process. A circularity of 1 and the desired filament diameter are always preferred. Any deviation from these values can result in over- or under-extrusion, leading to defects in the printed sample.

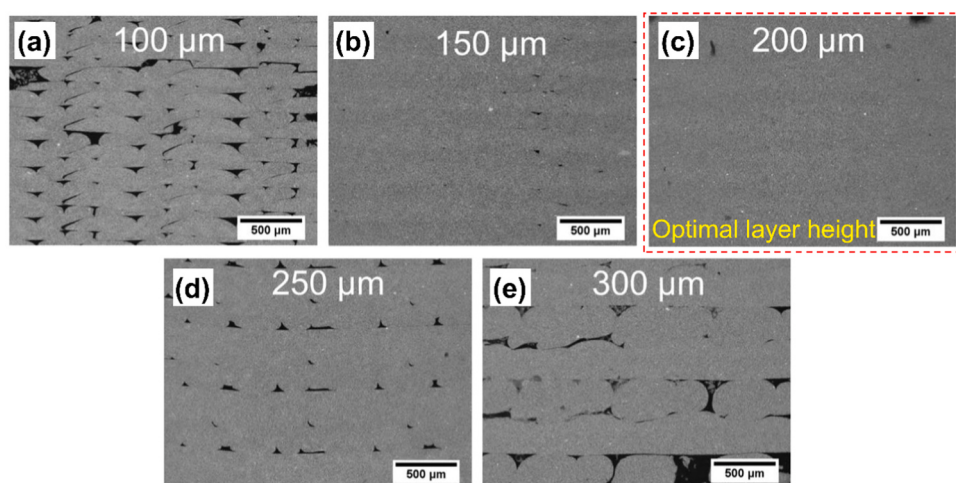


Fig. 15. Impact of layer height variation on the entrapped porosity. (a-e) Overview of SEM micrographs, depicting printing defects that occur at various layer thicknesses, ranging from 100 to 300 μm [107]. The optimal layer height has been marked in red dotted lines. (a-e) [107], Open access article distributed under the terms of the Creative Commons CC BY license.

(a-e) [107], Open access article distributed under the terms of the Creative Commons CC BY license.

2.3. Vat photopolymerization (VP)

2.3.1. Basics of the technology

Vat photopolymerization (VP) is an AM technique where a photocurable material in a vat is cured selectively by using a light source in the UV range. In the VP process, components are created layer-by-layer using stereolithography (SLA) or by projecting each complete layer using digital processing (DLP). This technique can be further classified according to the building direction of the fabricated component. In the top-down approach, the light source is positioned above the vat and the platform descends down to form the new layer. On the other hand, in the bottom-up approach, the light source is positioned below the vat and the platform ascends upward. A wiper blade is sometimes necessary to level the liquid surface before printing the subsequent layers, when using highly loaded ceramic slurries.

Among ceramic AM technologies, VP is known for its dimensional precision (mostly in the order of 10 – 50 µm, refer to Table 4), surface quality and ability to create intricate structures in miniature sizes. The success of printing using this technique heavily relies on the preparation of the slurry, which typically consists of a monomer or a mixture of different monomers, ceramic powder, dispersant, photo-initiators and photo-absorbers. In addition, it may also contain certain additives in form of diluents or pore-formers. Since ceramic particles are inert to light, polymerization only occurs in the organic monomer when exposed to light of certain frequency (usually 405 nm). So, the cross-linked monomers during the polymerization process uniformly surround the ceramic particles in each layer until the complete part is fabricated. The green components are then further processed by a high temperature treatment to completely remove the organics and obtain a high-density ceramic body.

There are certain requirements that need to be satisfied when using ceramic powders for such process. The ceramic suspension should have high solid loading (> 50 vol%) along with low viscosity (3000 mPa·s). Higher solid loading lowers the possibility of generating defects during the binder burn out process, thereby leading to high densities and better mechanical properties. On the other hand, low viscosities ensure that the ink can be spread easily and uniformly. So, there has to be a balance in terms of ceramic loading in the suspensions and the viscosity. An additional problem is related to the density of the ceramic powders. High-density powders (such as those of most piezoceramics) tend to sediment within the slurry, leading to the formation of layers of inhomogeneous ceramic content and defects in the parts after sintering. Another important issue that concerns piezoceramic powders is their high refractive index (RI) when compared to the base resin, as shown in Fig. 16. The difference in the RI affects the curing depth (C_d) and the resolution of the final component, due to scattering phenomena. For example, Song *et al.* compared the curing depth of ceramic suspensions involving three different powders, i.e. PZT, Zirconia (ZrO_2) and Alumina (Al_2O_3) with 65 wt% of ceramic loading and found out that ceramic suspensions with PZT powders exhibited the least curing depth of 39 µm when exposed for 10 s [134]. In contrast, suspensions with ZrO_2 and Al_2O_3 exhibited curing depths of 82 µm and 340 µm, respectively.

Considering the challenges related to VP of ceramic suspensions involving high RI powders such as piezoceramics, this section will review the important parameters that one needs to consider for preparing a printable ceramic suspension.

2.3.2. Effect of monomer

The monomer is the key component in the ceramic suspension that gives most photocurable resins their characteristic properties. Usually, monomers based on acrylates and methacrylates are most widely used [136] as evident from monomers reported in Table 4. Such monomers are activated only by free radicals from the photo-initiator [137]. In order to improve the adhesion between layers in the green body, it is crucial for the ceramic suspension to exhibit sufficient curing ability (at least greater than the slicing thickness). The curing depth (C_d) of the

photosensitive ceramic resin can be described by the equation [138]:

$$C_d = \frac{2d_{50}}{3\bar{Q}} \frac{n_0^2}{\Delta n^2} \ln\left(\frac{E_0}{E_c}\right) \quad (10)$$

where d_{50} is the average particle size of ceramic particles, \bar{Q} is the scattering efficiency term, Δn^2 is the square of the difference between the ceramic refractive index (n_p) and medium refractive index (n_0) [$\Delta n^2 = (n_p - n_0)^2$], E_0 is the energy density and E_c is the critical energy density (the minimum energy density required for photopolymerization). One can clearly observe from Eq. 10 that the curing depth is directly proportional to the intrinsic RI of the monomer and inversely proportional to the difference in the RI between the monomer and the piezoceramic particles. This suggests that a small increase in RI of the monomer can significantly increase the curing depth. For example, the RI of BT/PZT powders ($n_p \approx 2.4$) is significantly higher than that of the most commonly used acrylate resins ($n_0 \approx 1.4 - 1.6$) as shown in Fig. 16. As a result, Δn^2 is higher for suspensions containing such powders. In contrast, Al_2O_3 with a RI of 1.7 will possess a lower Δn^2 , hence denoting its strong curing ability.

To address this issue, Liu *et al.* compared the rheological and curing properties of 4 different monomers in a slurry containing 80 wt% of BT powders [139]. Among the monomers chosen for this investigation, acryloyl morpholine (ACMO) had the highest refractive index of 1.508, followed by polyethylene glycol diacrylate (PEGDA-1.466), 1,6-hexanediol diacrylate (HDDA-1.457) and tripropylene glycol diacrylate (TPGDA-1.450). The results indicate that the ACMO had the best curing capability among all the monomers used, followed by PEGDA (Fig. 17(a)), while HDDA and TPGDA with almost similar values of RI exhibited poor curing characteristics. This can be clearly correlated to Eq. 10. The Δn and n_0 for suspension containing ACMO is the least, hence resulting in enhanced curing performance. In a recent study, authors prepared a photocurable resin 40 vol% of BT with different monomers (4-hydroxybutyl acrylate (HBA), PEGDA, HDDA, TMPTA) and reported that TMPTA exhibited better curing capability (Fig. 17(b)) [140]. This is related to the number of functional groups present in the monomer; TMPTA has 3 acrylic groups with most carbon-carbon double bond and the highest RI among the other monomers. For similar reasons, Ma *et al.* selected PPTTA along with a combination of other monomers due to its higher functionality of 4 and refractive index [141].

In addition, rheological properties of the monomers should also be considered. Liu *et al.* found that PEGDA, with an inherent viscosity of 30 – 70 cps at 25 °C, exhibited the highest viscosity and shear thickening behaviour at high shear rates [139]. High viscosity can drastically decrease the printing efficiency. On the other hand, the other monomers exhibited shear-thinning behaviour, which is desired for such a printing process (Fig. 17(c)). However, ACMO was chosen considering the curing depth and the viscosity. In another study, HDDA was found to be the best monomer, outperforming others like TMPTA with a higher functionality, primarily because the suspension with HDDA had the lowest viscosity, allowing for easier and faster levelling (Fig. 17(d)) [140]. Dufaud *et al.* studied the stereolithography of PZT components using a mixture of two different photo-sensitive resins using DuPont Somos 6100 and HDDA [142]. Despite its higher refractive index of 1.52, Somos 6100 exhibited relatively high viscosity. Therefore, a blend containing Somos 6100 and HDDA was used to enhance photopolymerization, most likely with the goal of optimizing the viscosity for improved handling and printing while retaining ideal optical properties.

In recent years, there has been a trend toward developing ceramic suspensions that use several monomers in specified ratios to achieve highest performance [139,140,142–152]. However, with the exception of a couple of studies [144,146,151], no one has truly specified the precise ratios and the reason behind such formulations to the scientific community. There might be several reasons for this, but the most significant ones could be:

Table 4

Feedstock preparation and optimized printing parameters for vat photopolymerization.

Feedstock	Particle size and morphology	Photocurable monomer	Additives	Ceramic loading	Printing parameters			Reference
					UV wavelength (nm)	Exposure time (s)	Layer height (μm)	
BaTiO ₃	$d_{mean} = 1.27 \mu\text{m}$	HDDA	1-hydroxycyclohexyl phenyl ketone, Hypermer LP1, stearic acid, Triton X100, Zephrym 1000	0 – 55 vol%	350			Cured parts were dried for 24 h under UV light [154]
PZT	$d_{50} = 5 \mu\text{m}$	Diacryl 101, HDDA, Somos 6100, Dupont, RP-Cure 200, RPC	DMPA, Phosphoric ester, Irgacure 651	40 – 83 wt%		10, 25		[142]
PZT-5H		Diacrylate	2-propanol	$\geq 40 \text{ vol } \%$	260 – 550		20 – 40	Overnight drying at 50 °C [176]
PMNT		HDDA, DPPHA	Triton X-114, Irgacure 784	40 vol%	628, 519, 462		50	[177]
PZT 5 H		HDODA, Diacrylate		38 – 40 vol%				[178]
BaTiO ₃	100 nm	Photocurable resin SI500	Triton x-100	70 wt%				[179]
BaTiO ₃	APS = 1 μm	Photocurable resin SI500	Phospholan PS-131, Triton x-100	25 vol%		1 – 16	20	[168]
KNN		Acrylamide monomer	Triton x-100, TPO	65 wt% (31.9 vol %)	405		20	Inert film of Polydimethylsiloxane (PDMS) was coated on the vat surface to reduce the separation force [180]
BaTiO ₃	500 nm			70 – 86 wt%				[181]
PZT-5A		HDDA	BYK-142, TPO	34.1 – 48.7 vol %	385			[164]
BaTiO ₃	500 nm	HDDA, PEG(400)DA	BYK, TPO	40 vol%	405			Monomers in equal volume fraction [146]
BaTiO ₃	$d_{50} = 200 \text{ nm}, 500 \text{ nm}, 600 \text{ nm}$	PEGDA, HDDA	BYK, TPO	40 vol%			10	[147]
BaTiO ₃	$d_{50} = 993 \text{ nm}$	ACMO, PEG(400) DA, HDDA, TPGDA	Omnirad TPO, MEHQ, Triton x-100	65 – 82 wt%	405	10 – 180	30	[139]
PZT PMMA	1.5 μm 20 μm	TMPTA	Triton X-100, TPO	5 – 35 wt %	405	10 – 60	20	[171]
BaTiO ₃	Micron, $d_{50} = 3.4 \mu\text{m}$, Submicron, $d_{50} = 1.02 \mu\text{m}$, Nanoscale, $d_{50} = 50 – 70 \text{ nm}$	SG15 resin		70.1 wt % (30 vol %).	405	5 – 120	25, 50	Washed in absolute ethyl alcohol, Post curing 5 min in UV dryer [159]
BaTiO ₃	$d_{50} = 600 \text{ nm}$	OPPEOA, HDDA, TPGDA, EPTPA	TPO, Solisperse 41000	30 – 40 vol%	405		25	[148]
PZT	$d_{50} = 0.452 \mu\text{m}$	PEGDA	BAPO, BYK-142,	80 wt%	385	10 – 100		[170]
BaTiO ₃	$d_{50} = 136 \text{ nm}, 197 \text{ nm}, 355 \text{ nm}, 993 \text{ nm}, 1486 \text{ nm}$	ACMO	Triton X-100, Acrylic block copolymer, TPO, MEHQ	80 wt%	405	10 – 30	30	[157]
BCZT	$d_{50} = 1.7 \mu\text{m}$	OPPEOA, HDDA, TPGDA, EPTPA	Solisperse 41000, TPO	40 vol%			25	[149]
BaTiO ₃			DYSUPERBYK-100	37.14 – 51.82 vol %	465		10	[182]
KNNLN-Er PZT Soluble starch	$d_{50} = 0.8 \mu\text{m}$	ETPTA, OPPEOA, TPGDA, HDDA	BYK 9077, TPO Solisperse 41000, TPO	72 wt% 40 vol% 20 – 50 vol%				[183] [150]

(continued on next page)

Table 4 (continued)

Feedstock	Particle size and morphology	Photocurable monomer	Additives	Ceramic loading	Printing parameters			Reference
					UV wavelength (nm)	Exposure time (s)	Layer height (μm)	
PMN-PT	500 – 800 nm			77 wt%				[162]
BT templates	Length: 5 – 15 μm, Thickness: 0.5 – 1 μm			5 wt%				
BaTiO ₃	APS = 100 nm	PEG(400)DA, HDDA	Triton X–100, TPO	62 – 77 wt%	405		40	Monomers mixed in same volume ratio [151]
PZT	d ₅₀ = 0.452 μm	PEGDA	BAPO, BYK–142; PMMA	70 wt%	385	5 – 25		[174]
BaTiO ₃	Fine, d ₅₀ = 149 nm, Coarse, d ₅₀ = 879 nm	ACMO	TPO, MEHQ, Triton X–100, UNIQ FLOW 6057, UNIQ FOAM 7032	80 wt%	405	10 – 90	30	[158]
PZT Polystyrene	d ₅₀ = 0.8 μm 3 μm, 8 μm, 16 μm	OPPEOA, HDDA, TPGDA, ETPTA	Solsperse 41000, TPO, PEG–200, PS		405		25	[152]
BCZT			Solsperse 41000, TPO	40 vol%			25	[184]
BaTiO ₃	Micro powder, Nano powder	Acrylate-based photosensitive commercial resin	Triton X–100, TPO	20 – 50 wt%	405		25 – 100	[135]
BaTiO ₃	600 nm	OPPEOA, TPGDA, HDDA, ETPTA	Solsperse 41000, TPO	40 vol%	405			[163]
BT platelets	Width: 5 – 20 μm, Thickness: 1 – 2 μm			5 mol%				
PZT Polyethylene	d ₅₀ = 0.8 μm	OPPEOA, HDDA, TPGDA, ETPTA	Solsperse 41000, TPO, PEG–200, Polyethylene	30 – 60 vol%	405			[172]
BaTiO ₃	d ₅₀ = 200 nm	PUA, Acrylic ester, ACMO	DISPERBYK–111, TPO	65 – 80 wt%		5 – 35	20	[143]
KNN	d ₅₀ = 1.86 μm	HDDA, TMPTA	PEG200, Solsperse 41000, TPO	38 – 44 vol%	405		25	Monomers mixed in the mass ratio 5:4 [144]
BaTiO ₃ -xBaSnO ₃	1.99 – 3.4 μm	OPPEOA, HDDA, TPGDA, ETPTA	TPO, Solsperse 41000	40 vol%			25	[167]
PZT	d ₅₀ = 3 μm	SI500		65 wt%		10	20	[134]
BaTiO ₃		SI500		50 – 70 wt%	405	37	30	[185]
Barium acetate, titanium (IV) isopropoxide, acetic acid, acrylic acid		Ethoxylated trimethylolpropane triacrylate	TPO, Sudan Orange G		385	2	200	Samples washed with isoproponol [175]
PZT 5 H		HDDA, PEG, Polyurethane acrylate U600, Capryl alcohol		78 – 89 wt%		10	20	[186]
BaTiO ₃	<1 μm	Yellow dental clear	DISPERBYK–100	10 – 55 vol%	465		100	[187]
PZT855		PEGDA	Irg819	15 – 45 vol%			15	[188]
PZT Polystyrene	APS = 3 μm	HDDA, OPPEOA, ETPTA, TPGDA	Solsperse 41000, PEG–200, TPO				25	[145]
BaTiO ₃	d ₅₀ = 500 nm	HBA, PEGDA, HDDA, TMPTA	TPO, KOS110	40 vol%	405		10, 80	[140]
PZT	d ₅₀ = 0.452 μm	PEDGA	BAPO, DISPERBYK–142	70 wt%	405	10	10	[189]
PMMA	d ₅₀ = 5.86 μm							
BaTiO ₃	500 nm			75 – 85 wt%	405	9 – 27	30	[190]
Sm-PMN-PT	APS = 0.6 μm, 1.5 μm, 2.5 μm	HDDA, ACMO, OPPEA, PPTTA	PPG, POE, TPO, DISPERBYK–180	40 vol%	405	8, 30	25	[141]
BCZT		HDDA	TPO, DISPERBYK–110	45 – 55 vol%			25	[165]

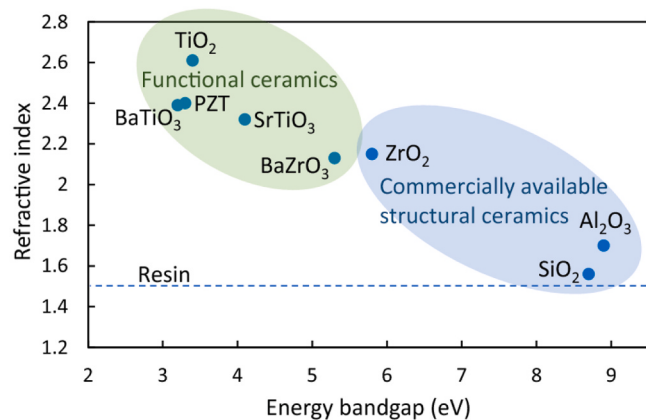


Fig. 16. Correlation between the energy bandgap and refractive index for different ceramic materials. The materials highlighted in green are of particular interest. The dashed line indicates the standard refractive index for a typical commercial resin [135]. [135], Open access article distributed under the terms of the Creative Commons CC BY license.

- (i) increasing the functionality to reduce the exposure time or the radiation energy required for curing,
- (ii) decreasing the viscosity,
- (iii) decreasing Δn by increasing the RI of the photocurable resin

Polyfunctional monomers such as dipentaerythritol penta/hexa-acrylate (DPPHA), or ethoxylated trimethylolpropane triacrylate (ETPTA) have multiple cross-linking sites when compared to HDDA or PEGDA which possess only two active cross-linking sites [153]. Such multiple-cross linking sites enable to form extensive and interconnected polymer networks, leading to enhanced green strength. Monomers such as HDDA can be used as a diluent because of their relatively low viscosity. Monomers with considerably higher RI, such as ACMO and oligo (propylene glycol) ethoxy triacrylate (OPPEOA), decrease the Δn of the overall ceramic suspension and this leads to a higher curing depth.

2.3.3. Effect of particle size

The particle size has a strong influence on the curing depth and the viscosity of the formulated suspension. It is quite evident from Eq. 10, that the curing depth increases with d_{50} . By maintaining a constant volume of solid particles, replacing fine particles with coarse particles reduces the scattering centres, leading to an increasing curing depth and a reduction in the over curing width. In this context, Jang *et al.* measured the reflectance of BT particles of two different sizes ($d_{mean} = 1.27 \mu\text{m}$ and

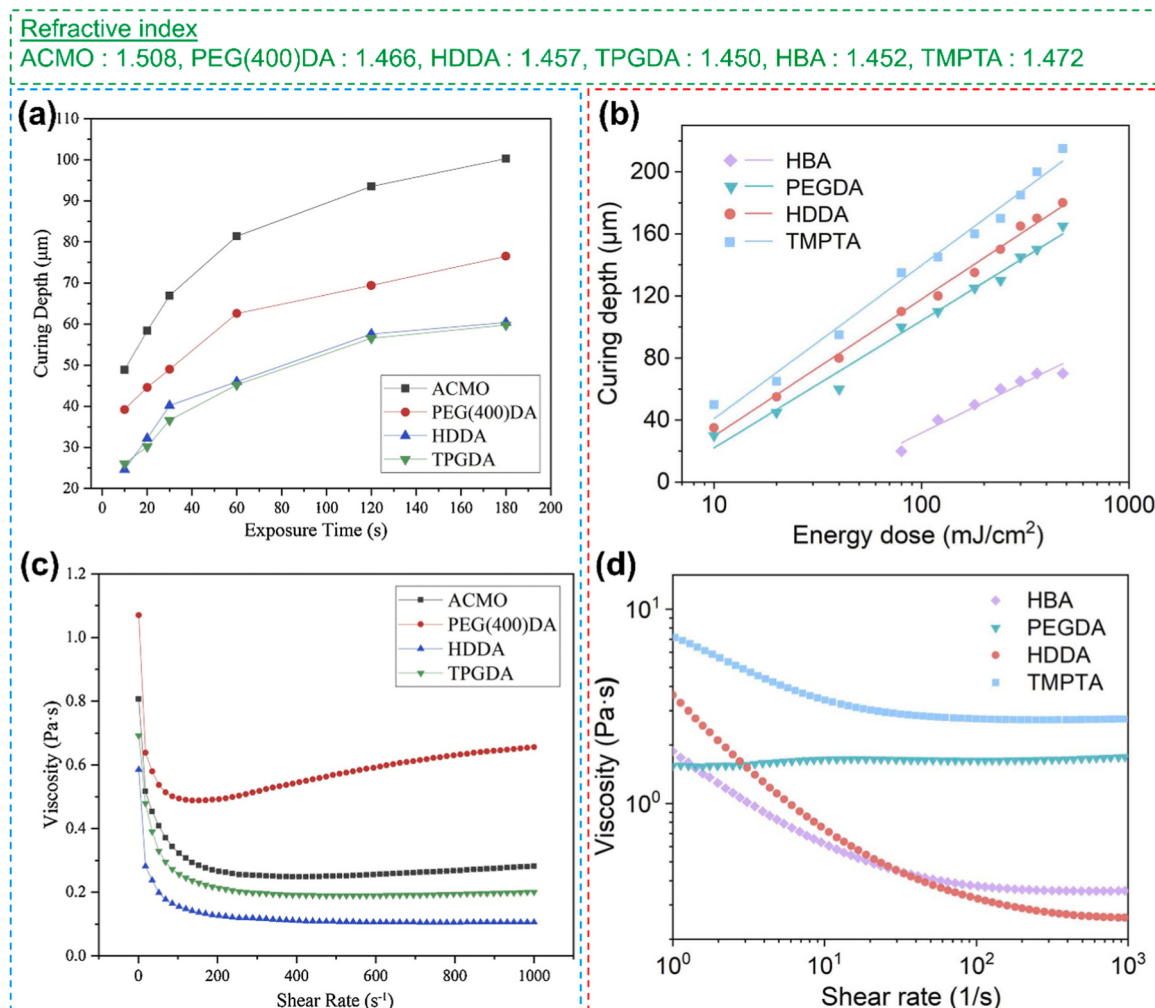


Fig. 17. Effect of the functionality and viscosity of different monomers for choosing the optimal one for the printing process. Curing and rheological properties of formulated with different monomers: Variation in curing depth as function of (a) Exposure time [139], and (b) Energy dose [140]. (c-d) Variation of viscosity with shear rate [139,140].

Reproduced from Ref.: (a, c) [139], and (b, d) [140] with permission from Elsevier

$2.09\text{ }\mu\text{m}$) in HDDA suspensions at varying solid loadings (10 vol% and 30 vol%) and reported that suspension with higher ceramic content and finer particle size exhibited increased reflectance due a large scattering centres, as shown in Fig. 18(a) [154]. Further, the suspensions with larger particle sizes exhibited a greater curing depth compared to suspensions with smaller particle sizes [141]. This was additionally corroborated by simulations conducted by Qin *et al.*, which predicted that finer particles would have greater scattering angles and lower penetration depths [155]. Conversely, fine particles can result in weak interfaces between layers, which becomes more pronounced after debinding and sintering [141].

Chen *et al.* compared the rheological and curing characteristics of BT suspensions (40 vol%) prepared with three different particles sizes (d_{50}) of 200, 500 and 600 nm [147]. The study revealed that the suspension containing coarse powder had the lowest viscosity, which is

advantageous in terms of self-leveling and recoating during the printing process. The suspensions with finer particles exhibited increased viscosity, due to high van der Waals forces causing them to strongly attract and clump together resulting in agglomeration (Fig. 18(b)). Nevertheless, all of the suspensions exhibited shear-thinning behaviour with viscosities well below 3000 mPa·s. This value is usually considered as an upper limit for a printable resin using conventional equipment [156]. Furthermore, the curing depth was analysed for all the suspensions and fitted according to Jacob's equation [136]:

$$C_d = D_p \ln\left(\frac{E_0}{E_c}\right); D_p = \frac{2d}{3\bar{\phi}Q} \quad (11)$$

where D_p is the attenuation length, d is the average particle size, $\bar{\phi}$ is the volume fraction of solids and \bar{Q} is the scattering efficiency. It was found that the curing depth increased with the applied energy dose (Fig. 18

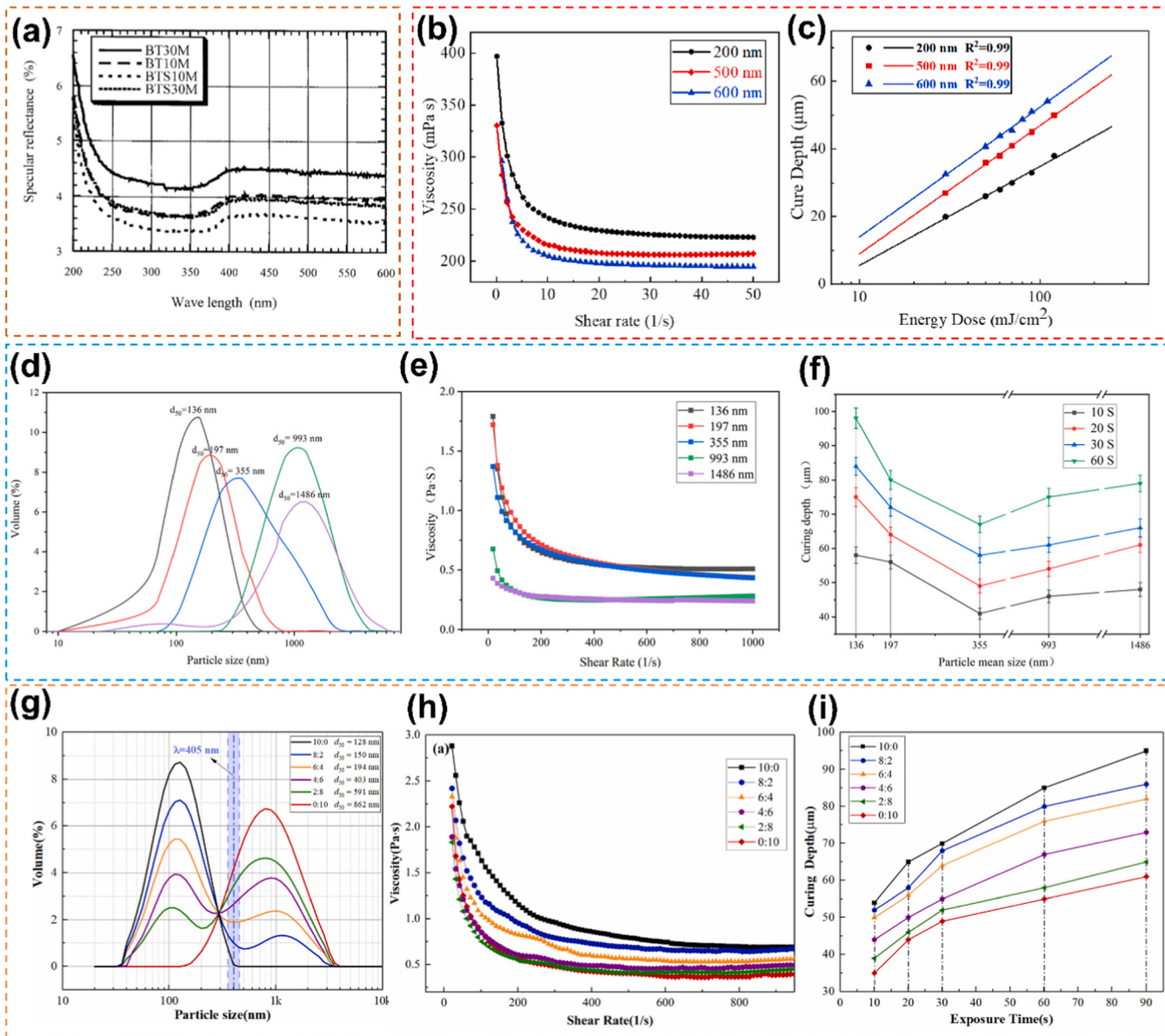


Fig. 18. Effect of the particle size and distribution on the viscosity and the curing behaviour. (a) Specular reflectance spectra of uncured BT-HDDA suspensions with mean particle sizes of $1.27\text{ }\mu\text{m}$ (denoted by BT) and $2.09\text{ }\mu\text{m}$ (denoted by BTS), with 10 vol% and 30 vol% ceramic powder [154]. (b) Viscosity as a function of shear rate, and (c) Dependence of curing depth and energy for different BT particle sizes [147]. (d) Particle size distribution, (e) Variation of viscosity, and (f) Curing properties of slurries containing ceramic powders with mean particle sizes of 136 nm, 197 nm, 355 nm, 993 nm, and 1486 nm [157]. (g) Particle size distribution, (h) Evolution of viscosity, and (i) Curing depth of BT ceramics in slurries at different particle size mass ratios [158].

Reproduced from Ref.: (a) [154], and (d-e) [157], with permission from John Wiley and Sons. (b-c) [147], and (f-h) [158], with permission from Elsevier.

(c)), which in accordance with Eq. 11. As a rule of thumb, the applied energy dose should be selected so that the cured thickness is at least double the slicing thickness to ensure better bonding between the layers.

Additionally, other investigations have also shown a similar relationship between viscosity and particle size [135,157,158]. In a recent study Liu *et al.* formulated inks with varying particle sizes (Fig. 18(d)), showing that the viscosity of 80 wt% BT decreased as the particle size increased to approximately 1 μm [157]. Further increasing the particle size to around 1.5 μm , the viscosity values almost saturated, indicating that particle size beyond this threshold value has no influence on the viscosity (Fig. 18(e)). Further, the relation between the curing depth and particle size was investigated for different exposure times. The results revealed that the curing depth increased with the exposure time. From Eq. 12, it can be observed that the curing depth is dependent on the median particle size and the scattering efficiency (\tilde{Q}), which is related to the particle spacing S (nm) and the UV wavelength λ (nm) using the equation [138]:

$$\tilde{Q} \propto \frac{S}{\lambda} \quad (12)$$

The results were quite surprising. With increasing particle size, the curing depth first decreased and then increased (Fig. 18(f)). However, one would expect that the curing depth should increase with increasing particle size. This is only valid for suspensions with relatively low solid loadings [156]. For highly concentrated ceramic slurries, the curing depth is strongly affected by the ratio of the inter-particle distance to the wavelength of light used for curing. When the particle size is smaller than the wavelength, typically $\lambda = 405 \text{ nm}$, the particles will tend to agglomerate due to strong inter-particle forces. This suggests that the value of \tilde{Q} decreases further with decreasing particle size and is inversely related to the curing depth. In other words, \tilde{Q} increases with increasing particle size and the curing depth decreases. On the other hand, when the particle size is greater than 405 nm, the tendency to agglomeration decreases. Hence the inter-particle spacing increases and the particle characteristics become dominant compared to scattering. As a result, the curing depth increases. However, despite the fact that the curing depth improves as the particle size exceeds 405 nm, it does not exceed the curing depth achieved with smaller particles under identical exposure duration. For instance, the curing depth for suspensions containing 1.5 μm particles was 80 μm , whereas that with 136 nm particles was 100 μm , with both suspensions being exposed for 60 s.

Liu *et al.* prepared ceramic suspensions by incorporating two distinct BT powders with average particle sizes (d_{50}) of 149 and 879 nm in different ratios (Fig. 18(g)), respectively, at a ceramic loading of 80 wt% [158]. The curing depth (and viscosity) was strongly related to the particle size; both of them decreased with increasing amount of coarser particles (Fig. 18(h-i)). This is due to the fact that when the weight proportion of the coarser particles increased, the proportion of particles with sizes near the UV wavelength also increased, as marked in Fig. 18(g). Consequently, this leads to an increase in scattering and a reduction in the curing depth. The closer the particle size is to the UV wavelength, the greater the scattering.

Sotov *et al.* prepared ceramic suspensions with 70.1 wt% of BT using different particle sizes (micron-sized = 3.4 μm , sub-micron = 1.02 μm , nano-sized = 50 – 70 nm) [159]. The viscosity of the suspensions with micron and sub-micron sized particles were well within the widely accepted value of 3000 mPa·s. In contrast, the suspension with nano-particles possessed extremely high viscosity values. Due to the high viscosity, recoating of the slurry using the scraper blade resulted in an uneven surface. As a result, such suspensions were ruled out for further use. Moreover, the suspensions prepared with micron-sized particles ($d_{10} = 0.1 \mu\text{m}$, $d_{50} = 3.4 \mu\text{m}$, $d_{90} = 25.4 \mu\text{m}$) resulted in delamination of the printed samples. This was attributed to the presence of larger particles which lead to weak adhesion of the layers. The suspensions with sub-micron sized particles were the best in terms of

printing accuracy.

2.3.4. Platelets orientation

Generally, textured piezoceramics exhibit better properties when compared to the non-textured counterparts and are obtained by a process called templated grain growth. It is to be noted that platelet alignment and induced grain-growth by thermal treatment are the two important factors that determine the final texture. However, the main concern here is the alignment of these platelets during the printing process.

The platelet alignment during the printing is a crucial step that influences the final degree of texture. Such texturing can be only obtained with printers that employ a doctor blade to level-off the slurry after each layer has been printed. The doctor blade aligns the platelets by exerting sufficient shear forces. The extent to which texturing can be achieved in the green bodies depends on the ratio of the pressure-driven forces to the slurry-driven force and it can be written as [160,161]:

$$\Pi = \frac{\Delta PH^2}{2\mu t_{blade} U} = \frac{\text{pressure - driven forces}}{\text{slurry - driven forces}} \quad (13)$$

$$\Delta P = \rho_{slurry} g H_{slurry} \quad (14)$$

where ΔP is the pressure exerted by the slurry head, H is the blade gap, μ is the slurry viscosity, t_{blade} is the thickness of the doctor blade, U is the carrier velocity, ρ_{slurry} is the density of the slurry, H_{slurry} is the height of slurry. A lower value of this ratio (Π) yields a better alignment. One can clearly observe from Eq. 13, that the alignment is completely dependent on the printing parameters, provided that the platelets concentration is sufficient.

Zhang *et al.* prepared ceramic suspensions using PMN-PT ceramics with 5 wt% of (001)-BT platelets to provide sufficient evidence that stereolithography is similar to the tape casting process, but with more benefits associated [162]. In order to minimize the ratio as mentioned in Eq. 13, a ceramic loading of 77 wt% with a blade gap of 30 μm was chosen as the best parameter. The platelet alignment in the polymer-ceramic matrix was confirmed by cross-sectional SEM observations which revealed an average deviation angle of 11.77°.

In a more recent study, Du *et al.* employed different amounts of <001> oriented BT platelets in a BT slurry with solid loadings of 40 vol %. 5 mol% of platelets were chosen as the optimal concentration [163]. Further increasing platelet concentration hindered the parallel alignment of the platelets. The height of the scraper blade was determined to be 100 – 125 μm . Increasing the height of the scraper blade subsequently decreased the shear forces acting on the platelets. It is important to mention here that the optimized concentration was decided after analysing the X-ray diffraction (XRD) pattern of the sintered components produced with different processing parameters.

2.3.5. Effect of ceramic loading

Higher ceramic loadings in the slurry ensures better properties in terms of better density, minimized residual porosity and reduced defects after the binder burn out and sintering process. In general, the viscosities of ceramic suspensions increase with increasing ceramic loading and their shear-thinning behaviour becomes more pronounced, as evidenced by numerous studies [135,142,144,159,164,165].

In a recent study, Stefan *et al.* characterized the rheology of slurries with different ceramic content of BT. Up to solid loadings of 40 vol%, the viscosities remained unaffected by the shear rates (Fig. 19(a)), suggesting a strong Newtonian behaviour ($n = 1$) [135]. This was further confirmed by determining the power law parameter (n), which resulted in the range of 0.95 – 1.08, which is close to 1. With further increasing the solid loading to 45 vol%, the viscosity drastically increased by around two folds and displayed a strong shear thinning behaviour. However, since the viscosity of all the prepared ceramic suspensions were well below the standard value of 3000 mPa·s [156], it was

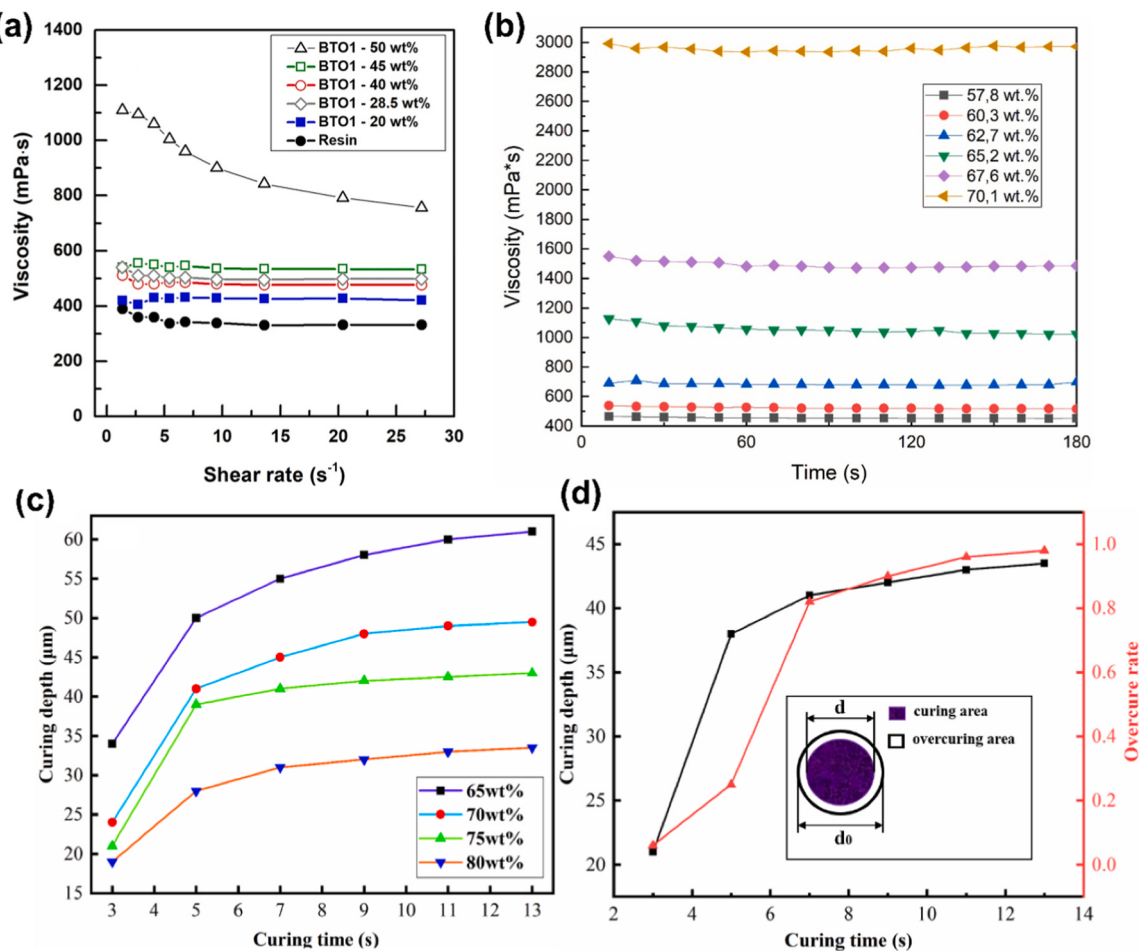


Fig. 19. Effect of the ceramic loading on the viscosity and curing depth. (a) Viscosity as a function of shear rate for ceramic resins containing different weight fractions of BT powder [135]. (b) Evolution of the ink viscosity with different BT solid loadings over varying measurement times, exhibiting the stability [159]. (c) Variation of the curing depth as a function of the curing time for varying ceramic loadings [143]. (d) Curing depth and over-curing rate as a function of curing time for a ceramic loading of 75 wt% [143].

(a) [135], (c-d) [143] Open access article distributed under the terms of the Creative Commons CC BY license. Reproduced from Ref.: (b) [159], with permission from Elsevier.

considered suitable for printing.

In addition to the viscosity, the stability of the slurry is important which needs to be taken care of. In an ideal situation, the viscosity should remain constant as a function of time. This is in good agreement with the results reported by Sotov *et al.* (Fig. 19(b)) [159]. This means that the ceramic particles are well dispersed and there is no sedimentation in the prepared ink. However, the results reported in Fig. 19(b) describe the stability only for a short period of time. For low-cost printers, a scraper blade may not be present and, in that case, it is advisable to assess the stability of the slurry over an extended duration of time.

As indicated by Eq. 11, the curing depth is inversely proportional to the volumetric ceramic content in the suspension. The greater the ceramic content, the more the particles act as scattering centres for light. This was also demonstrated by reflectance measurements conducted by Jang *et al.* on suspensions containing 10 vol% and 30 vol% of piezo-ceramic particles (Fig. 18(a)) [154]. Conversely, slurries with extremely low ceramic content exhibit an increase in curing depth. However, this comes at the expense of post-processing complexities, such as high shrinkage and cracking after the thermal treatment. Note that the scattering causes the UV radiation to propagate in a different direction. This results in an increasing curing width perpendicular to the incident light and in a decrease in the curing depth in the direction of the incident light [166]. The best compromise is to optimize the balance between

ceramic content and the curing time in order to reduce the over-curing width. It is important to note that the curing depth determines the vertical resolution, while the curing width determines the lateral resolution. Moreover, the additions of dopants significantly affect the physical properties of the ceramic powders such as the RI and density [167]. So, it is necessary to understand the curing behaviour of such doped powders for reliable printing.

In this context, Zhang *et al.* investigated the curing depth and over-curing rate as a function of ceramic loading and exposure time [143]. It was found that curing depth increased with exposure time and with prolonged exposure the over-curing width also increased (Fig. 19(c-d)). The best compromise was achieved by using solid loadings of 75 wt% with a curing time of 5 s. This resulted in the desired curing depth with decreased width of over-curing. Similar reports on the effect of curing depth by varying the ceramic loadings has been reported elsewhere [135,144,168].

2.3.6. Effect of dispersant concentration

Dispersants are often used for several reasons, including the stabilization of ceramic suspensions, breaking up of agglomerates and the prevention of sedimentation. In general, the amount of dispersant should be proportional to the surface area of the ceramic powders. This is because adsorption is a surface effect. However, the concentration should be adjusted when the volumetric fractions of ceramic powder

increases.

In this regard, Wang *et al.* thoroughly investigated the viscosity of 15 vol% BT with concentration of dispersant ranging from 0.3 wt% to 8 wt% [146]. The optimal dispersant concentration was reported to be 1 wt% (Fig. 20(a)). There usually exists an optimum concentration of the dispersant that leads to the lowest viscosity. Inadequate amount of dispersant may result in insufficient covering of particle surfaces, hence leading to agglomeration and high viscosity. On the contrary, excess dispersant is reported to degrade the rheological characteristics of the suspension. The excess dispersant moves freely inside the slurry and leads to depletion flocculation, a condition in which the inter-particle distance decreases, thereby enhancing the agglomeration and viscosity of the suspension. Several researchers have optimized the dispersant concentration by carefully observing the variation of viscosity at higher shear rates ($\geq 40 \text{ s}^{-1}$) [144,149,169].

Kim *et al.* reported a detailed investigation on the influence of dispersant concentration (1 wt%, 2 wt%, 3 wt%) on the rheological behaviour and the curing properties of a PZT suspension [170]. Initially, Fourier transform infrared spectroscopy (FTIR) analysis revealed that the optimum dispersant concentration was either 2 wt% or 3 wt% based on the degree of adsorption of the dispersant to the ceramic particles. The flow curves revealed that the suspension with 2 wt% of dispersants had the least viscosity with strongest shear-thinning behaviour ($n = 0.19217$ compared to 0.46280 for 3 wt% and 0.82873 for 1 wt%) (Fig. 20(b)). Further, the dispersion stability of the suspension was measured by a dispersion stability analyser. Since sedimentation is most favoured for the particles in the upper part of the size scale, this region was considered for the stability measurements. The backscattering intensity as a function of time (72 h) decreased for all suspensions, indicating that some sort of sedimentation occurred (Fig. 20(c)). The suspensions with 1 and 3 wt% of dispersant exhibited almost similar backscattered intensity (≈ -46), with the latter exhibiting a non-linear/abrupt decrease. In contrast, the suspension with 1 wt% of dispersant exhibited a value of -35 . This lower value indicates that the sedimentation rate was lower when compared to the others. The dispersion stability was further quantified using the Turbiscan stability index (TSI). These results emphasize that the suspension with 2 wt% of dispersant was the best overall choice.

In further experiments, the curing ability was measured using a photo-calorimetry and the results revealed that the suspension with 2 wt % dispersant exhibited the highest polymerization rate of 0.085 s^{-1} and a maximum conversion of 43 % among all suspensions (Fig. 20(d)). In order to analyse the effect of the dispersant on the curing depth, a circle of $1000 \mu\text{m}$ was used as a reference. The curing depth increased with applied energy. However, no correlation between dispersant concentration and curing depth could be identified at this time. This can be due to differently dispersed or flocculated states of the powder. The surface of the printed circles was investigated with the help of SEM (Fig. 20(e)) and the suspension with 2 wt% of dispersants had the smallest average particle size of 352 nm . In comparison, for the suspensions containing 1 and 3 wt% dispersants the smallest average particle size was 675 and 553 nm , respectively. This variation in the average particle size has a considerable impact on the surface roughness of the printed component. The samples were quantified by two roughness parameters namely, R_a and S_a . Both parameters exhibited similar trends, even though some difference existed in the numerical value. The most significant outcome was that the solution containing 2 wt% of dispersants, regardless of the curing parameters, showed the lowest levels of R_a and S_a , corresponding to a better surface finish. By correlating both the curing depth and the surface roughness, a revised curing depth parameter (C_d') was plotted (Fig. 20(f)). The findings indicate that suspensions containing 2 wt% and 3 wt% of dispersants were suitable for achieving a high curing depth, hence enhancing inter-layer adhesion. The revised curing depth curve was fitted with the Jacobs equation (Eq. 11), in order to calculate D_p and E_c . Interestingly, the suspension with 2 wt% of dispersants had

the lowest D_p and E_c values. The decrease in the depth of curing may be related to the comparable values of the wavelength of UV radiation used for curing (385 nm) and the particle size (352 nm) of the suspension with 2 wt% of dispersants. The scattering effect is prominent at such conditions and can decrease the curing depth drastically. However, having the smallest E_c is desirable as it suppresses the scattering and leads to a high printing accuracy, with decreased value of over-curing width. Finally, the over-curing width measurements pointed out that the suspension with 2 wt% of dispersants showed the lowest value (Fig. 20(g)).

2.3.7. Effect of photo-initiator (PI) concentration

Low molecular weight organic photo-initiators are sensitive to the UV light and produce free radicals that can attack the functional sites of the photocurable resins or monomers. Most of the acrylate monomers are activated using free radical photo-initiators (PI). The amount of PI used should be in proportion to the total amount of monomer used in the formulation. For the best curing properties, an optimum amount of PI is desired; deviation from this amount leads to degradation in the curing ability.

The inherent curing ability of the ceramic suspension is dictated by the amount of PI present in the suspension. Liu *et al.* investigated the effect of using different PI concentrations (TPO: 1 wt%, 2 wt%, 3 wt%, 4 wt%, 5 wt%) on the curing depth of suspensions containing 40 vol% of BT [148]. An energy dose of 160 mJ/cm^2 was chosen since the curing depth ($50 \mu\text{m}$) was at least double the slicing thickness ($25 \mu\text{m}$). Initially, the curing depth increased with the TPO concentration up to 3 wt%. However, beyond such optimum concentration, the cured depth decreased (Fig. 21(a-b)). This is in good agreement with a recent study [167]. The TPO absorbs the incident UV light and generates free radicals. The higher the concentration of TPO, the more radicals are generated, thereby increasing the curing depth until the optimum concentration is reached. On further increasing the concentration, the freely moving TPO in the slurry can absorb the UV radiation, generating more free radicals that can lead to a chain termination reaction between the free radical and the acrylate monomer, or decrease the reactivity by recombination of the free radicals. As a result, a decrease in the curing depth was observed on using excessive PI.

Almost similar observations were reported by He *et al.* for a 40 vol% BCZT suspension [149]. However, beyond the optimum concentration of TPO (3 wt%), the curing depth did not exhibit any dependency on the TPO content (Fig. 21(c)). The variation of the curing depth with the applied energy dose was plotted to understand the D_p and E_c (Fig. 21(d)). The slope of the curves is essentially identical, suggesting that the photo-initiator concentration has little impact on the attenuation length, D_p . However, with the increasing concentration of TPO, E_c decreased from 5.58 to 5.10 mJ/cm^2 , suggesting a lower energy dose is required to initiate polymerization. Finally, a TPO content of 3 wt% with an energy dose of 40 mJ/cm^2 were chosen as the optimum values for a layer thickness of $25 \mu\text{m}$. In a recent study, Pan *et al.* reported that the optimum TPO concentration for a suspension containing 42 vol% of KNN was 1.5 wt% with an exposure energy of 29 mJ/cm^2 for fabricating samples with a layer thickness of $25 \mu\text{m}$ [144]. In conclusion, high PI concentration can lead to an increasing over-curing width and low printing accuracy.

2.3.8. Effect of using additives with low RI

It is clear that ceramic suspensions containing piezoceramic powders suffer from low curing depth and severe scattering because of the higher refractive index (RI) of the particles with respect to that of the most commonly used acrylate monomers. One effective way to solve this issue is the addition of materials with low RI and high UV absorptivity to the suspensions. Replacing the piezoceramic powder by materials such as polystyrene (PS), polyethylene (PE), polymethyl methacrylate (PMMA) and soluble starch (SS) will decrease Δn^2 in Eq. 10, leading to enhanced